Insolation forcing of coccolithophore productivity in the North Atlantic during the Middle Pleistocene

C. Cavaleiro[1, 2, 3], A. H. L. Voelker[2, 3], H. Stoll[4*], K.-H. Baumann[1, 5], D. K. Kulhanek[6], B. D. A. Naafs[7], R. Stein[8], J. Grützner[8], C. Ventura[2], and M. Kucera[1]

[1] University of Bremen, MARUM - Center for Marine and Environmental Sciences, Leobener Straße 28359, Germany.

[2] IPMA – Instituto Português do Mar e da Atmosfera, Divisão de Geologia Marinha e Georrecursos Marinhos, Rua Alfredo Magalhães Ramalho 6, 1495-006 Lisboa, Portugal.

[3] CCMAR, Centro de Ciências do Mar, Universidade do Algarve, Campus de Gambelas, 8005-139 Faro, Portugal.

[4] Geology Department, University of Oviedo, C/. Jesús Arias de Velasco s/n, 33005, Oviedo, Spain.

[5] University of Bremen, Geosciences Department, Klagenfurter Straße, 28359 Bremen, Germany.

[6] International Ocean Discovery Program, Texas A&M University, College Station, Texas 77845-9547, USA.

[7] Organic Geochemistry Unit, School of Chemistry, Cabot Institute, University of Bristol, Cantock's Close, Bristol BS8 1TS, UK.

[8] Alfred-Wegener Institute for Polar and Marine Research, Am Alten Hafen 26, 27568 Bremerhaven, Germany.

Corresponding author: Catarina Cavaleiro (cdcavaleiro@gmail.com)

*now at: Department of Earth Sciences, ETH Zürich, Sonneggstrasse 5. 8092 Zürich, Switzerland

Key Words:

Pleistocene

North Atlantic

Coccolithophores

Paleoproductivity

Insolation

Glacials

Highlights (85 characters max. including spaces):

- Coccolithophore productivity is higher during glacials.
- Coccolithophores adjust their phenology in response to insolation forcing.
- Enhanced productivity occurs when summer/autumn insolation is at its maximum.

Abstract

Coccolithophores play a key role in the oceanic carbon cycle through the biological and carbonate pumps. Understanding controls on coccolithophore productivity is thus fundamental to quantify oceanic carbon cycling. We investigate changes in coccolithophore productivity over several Pleistocene glacial-interglacial cycles using a high-resolution coccolith Sr/Ca ratio record, which is an indicator of growth rate and thus a proxy for coccolithophore productivity. We use Middle Pleistocene sediments from the North Atlantic Integrated Ocean Drilling Program (IODP) Site U1313 (41.00' N, 32.58' W) spanning Marine Isotopic Stages 16 to 10 (638 to 356 kyr). The location of the record allows us to investigate processes affecting productivity in a mid-latitude setting and to unravel the effects of temperature and regional ocean circulation. Coccolithophore productivity shows a dominant glacial-interglacial cyclicity with higher productivity during glacials, which appears to reflect the southward migration of the North Atlantic high productivity zone currently located between 45º and 55º N. Spectral analysis of the productivity record reveals a suborbital variability consistent with forcing by insolation maxima superimposed on the front migration pattern. Similar to today, coccolithophore productivity during interglacials was enhanced when insolation was at its maximum in spring or in autumn, whereas during glacials, productivity was enhanced when summer/autumn insolation was at its maximum. We show that in the studied region, coccolithophore productivity was driven by processes reflecting regional insolation. Applying this information to model experiments is required to assess if coccolithophore productivity played a significant role in past changes of atmospheric CO_2.

1. Introduction

Coccolithophores are the main primary producers in temperate regions of the open ocean (Brand, 1994) producing biogenic calcite (Bolton et al., 2016) and mediating cycling, sequestration and export of organic and inorganic carbon (Rost and Riebesell, 2004; Baumann et al., 2005). Coccoliths, the minute calcite plates that cover coccolithophore cell, are very abundant in seafloor sediments and have been extensively used as paleoenvironmental tracers providing information on paleoceanographic conditions and composition of the overlying photic zone's communities (e.g., Flores et al., 2003; Baumann et al., 2005; Marino et al., 2014; Emanuele et al., 2015; Maiorano et al., 2015). Enhanced coccolithophore calcification during glacials and terminations has been suggested to drive a decrease in the availability of the carbonate ion in the ocean and trigger the deglacial rise in atmospheric carbon dioxide (pCO_2) (Rickaby et al., 2010; Omta et al., 2013). Reconstructing past variations in the production and accumulation of sedimentary carbonate is thus important for understanding changes in pCO_2 (Sigman et al., 1998; Sigman and Boyle, 2000).

In well-preserved sediments, coccolithophore productivity has commonly been inferred from the total coccolith abundance (e.g., Emanuele et al., 2015) and the nannofossil accumulation rate (NAR) (e.g., Flores and Sierro, 2007; Cabarcos et al., 2014), but also from the relative abundance of small placoliths and *Florisphaera profunda* (e.g., Marino et al., 2008). In addition, other primary production indicators, such as alkenones (organic molecules mostly produced by certain species of coccolithophores) are also used (e.g., Villanueva et al., 2001; Emanuele et al., 2015). The accumulation of organic matter, including total organic carbon (TOC) and alkenones, represents the most direct record of general and coccolithophore productivity, respectively (Schoepfer et al., 2015). Both have been used as paleo-productivity

proxies (e.g., Rühlemann et al., 1999; Stein et al., 2009) by assuming that changes in organic carbon content of sediment can be interpreted as changes in the surface productivity through time (Wefer et al., 1999). However, all of these proxies depend not only on supply but also on dilution (by minerals or other sediment constituents), sedimentation or accumulation rates, and preservation conditions (Rullkötter, 2006).

The coccolith fraction (CF) Sr/Ca ratio has been suggested as an alternative productivity proxy that is independent of accumulation rate. Coccolithophores construct coccoliths internally within their cell and several studies suggest that Sr/Ca of the coccolith is directly proportional to the coccolith calcification rate, which is a function of growth rate (e.g., Stoll and Schrag, 2000; Rickaby et al., 2007; Mejía et al., 2014). The faster coccolithophores grow, the faster they calcify and the more Sr is incorporated into the calcite lattice of their coccoliths (Stoll and Schrag, 2000; Stoll et al., 2002a).

The amount of Sr introduced into the calcite (Sr partitioning) varies among genera and species, with larger and more heavily calcified coccoliths generally having higher Sr content than smaller and lighter coccoliths (Stoll et al., 2007; Fink et al., 2010). Dissolution intensity and changes in coccolith assemblage appear to exert only a minor influence on CF Sr/Ca in the modern ocean (Stoll and Schrag, 2000). However, significant downcore changes in coccolith assemblages, including due to intensive or selective dissolution (Stoll et al., 2002b), should be evaluated when applying this proxy to the past.

In laboratory cultures, coccolith Sr/Ca also correlates with temperature. Stoll et al. (2002a) cultured different coccolithophore species strains at different temperatures, with results for several strains of *Gephyrocapsa oceanica* indicating that increasing temperature can increase Sr partitioning. This suggests that there is a temperature-controlled change in Sr partitioning

coefficients (D_{Sr}) in calcite, analogous to that observed in abiogenic dolomite-calcite and aragonite-calcite transformation experiments (Malone and Baker, 1999). If this interpretation is correct, then the temperature effect should be removed from coccolith Sr/Ca records to identify the component of variation due to growth rate. If the temperature effect on D_{Sr} is the dominant source of temperature dependence on coccolith Sr/Ca in culture experiments (Stoll et al., 2002a; Müller et al., 2014), then the relationship from cultures coupled with an independent temperature measurement (e.g., Mg/Ca-based sea-surface temperature (SST) from foraminifers) can be used to correct for this effect, as has been done in previous studies (e.g., Mejía et al., 2014). With temperature and assemblage effects considered, the SST corrected CF Sr/Ca curve should mostly reflect qualitatively coccolithophore growth rate and therefore their productivity (Stoll et al., 2002a; Müller et al., 2014). The validity of the CF Sr/Ca productivity proxy has been established in previous studies in oceanographic regions where SST variations over glacial-interglacial cycles were relatively small (~4 - 6ºC) (Mejía et al., 2014; Tangunan et al., 2017) as well as in the Southern Ocean where SSTs are significantly lower (varying between 6 ºC - 12 ºC) (Saavedra-Pellitero et al., 2017).

Here, we reconstruct the paleoproductivity of coccolithophores, the most significant component of the phytoplankton community in the central North Atlantic, based on the CF Sr/Ca ratio. We used a carbonate-rich sediment archive that contains well-preserved coccolithophores from the mid-latitude North Atlantic (IODP Site U1313), spanning the mid-Brunhes dissolution interval and the *Gephyrocapsa caribbeanica* acme (e.g., Baumann and Freitag, 2004; Barker et al., 2006). The location of IODP Site U1313 (Fig. 1) allows the assessment of coccolithophore productivity changes in a transitional productivity area particularly sensitive to basin-scale forcing changes, such as changes in temperature and circulation (Barton et al., 2003).

125

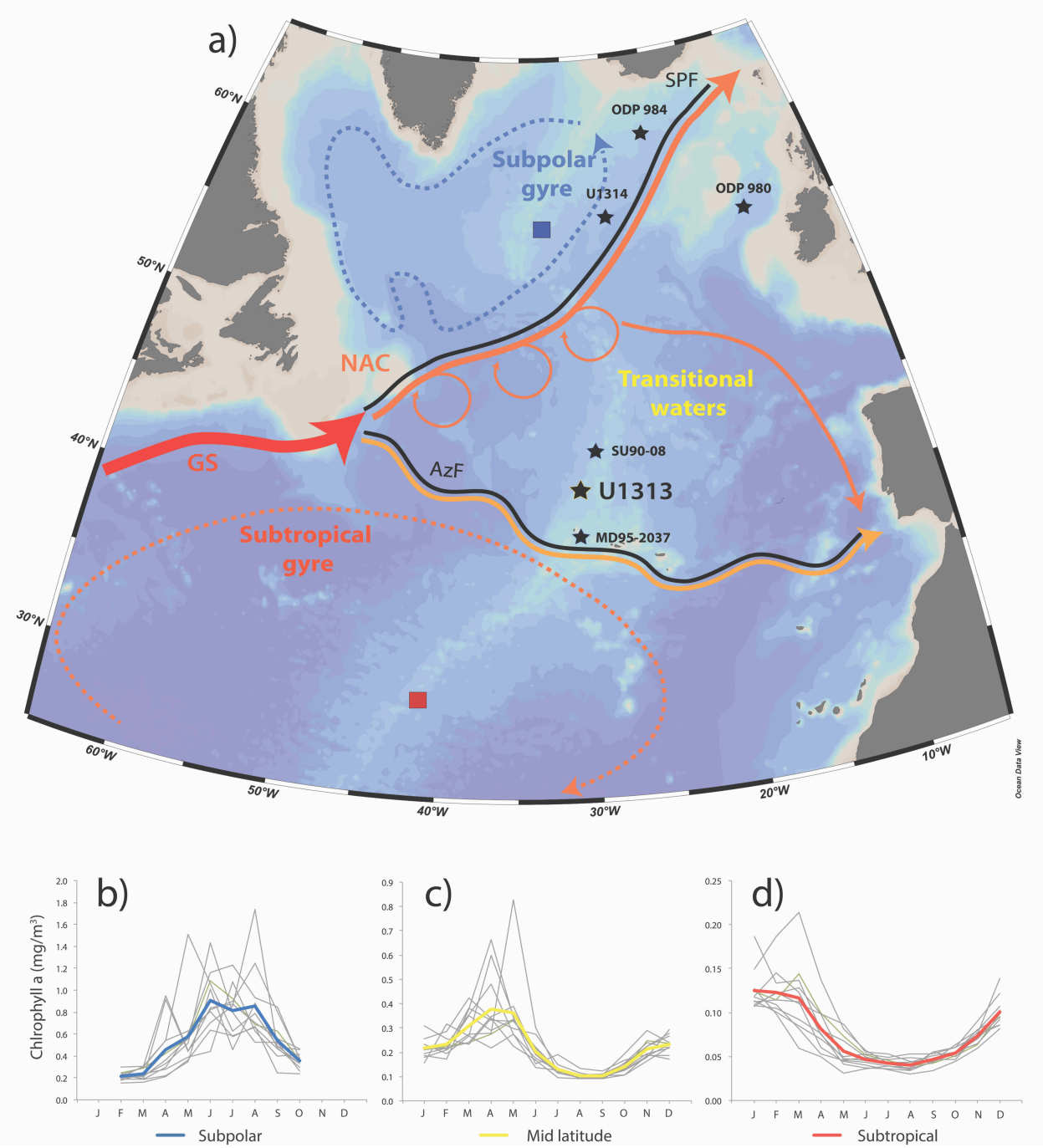

126

127 Fig. 1 - Study area: (a) Schematic surface ocean circulation of the North Atlantic, in the vicinity of IODP Site U1313. Major
128 currents and oceanic fronts: Gulf Stream (GS, in red), North Atlantic Current (NAC, in dark orange), Azores Current (AC, in
129 light orange); and associated fronts: Subpolar Front (SPF) and Azores Front (AzF) – both as black lines. Black stars evidence
130 sediment data: IODP Site U1313 (this study), IODP Site U1314 (Alonso-Garcia et al. 2011), ODP Site 980 and 984 (*Oppo et al.*,

1998 and Ortiz et al., 1999, respectively), cores SU90-08 and MD95-2037 (*Villanueva et al.*, 2001). Map template made with Ocean Data View (*Schlitzer*, 2015). Note different scales of the monthly chlorophyll *a* concentration represented in (b), (c) and (d) for the different production regimes, respectively: (b) subpolar (represented by the blue square located at 55 - 57º N, 31 - 33º W), (c) for the mid-latitude (black star at the location of IODP Site U1313, 40 - 42º N, 31 - 33º W) and (d) for the subtropical production regimes (red square located at 30 - 32º N, 41 - 43º W). Blue, yellow and red heavy lines indicate an average of ten years for each regime, respectively, whereas grey lines are individual years (2003 to 2013). Chlorophyll *a* concentration derived from MODIS and SeaWiFS satellite data available at http://disc.sci.gsfc.nasa.gov/giovanni).

The key motivation for this study is to understand the climate drivers of North Atlantic coccolithophore production dynamics across Pleistocene glacial/interglacial cycles. We investigate how atmospheric and hydrographic changes influence coccolithophore productivity, at both orbital and suborbital time scales. We emphasize that our research focuses on the qualitative characteristics of the paleoproductivity record, namely the inherent orbital and suborbital periodicities, rather than quantitatively estimating the coccolithophore productivity. Thus, we reconstruct the CF Sr/Ca component of coccolithophore productivity and not quantitative production.

We analyze changes in the ocean surface circulation and its relationship to nutrient availability, as well as changes in the insolation as a potential forcing mechanism. To do this we reconstructed coccolithophore productivity qualitatively based on the CF Sr/Ca at IODP Site U1313 over the interval between 638 and 356 ka. This is the first time that the Sr/Ca proxy has been used in a temperate region that experienced significant SST oscillations associated with glacial ice-rafting events (Stein et al., 2009; Naafs et al., 2011) and we address potential caveats accordingly. The studied interval covers a wide range of climatic conditions from Marine Isotopic Stages (MIS) 15 to MIS 11, including the late and early phases of MIS 16 and MIS 10, respectively. MIS 11 is acknowledged as an analogue for the present interglacial (e.g., Loutre and Berger, 2003) and MIS 12 was one of the harshest glacials of the last one million years (e.g.,

156 Jansen et al., 1986). On the other hand, MIS 15 and MIS 13, on the other hand, were relatively
157 milder interglacial stages than MIS 11 (Jouzel et al., 2007).

158 It is worth noting that coccolithophore communities evolved and changed throughout this
159 interval (e.g. Bollmann et al., 1998). Our 300 kyr-long sedimentary record falls mostly within the
160 *Gephyrocapsa caribbeanica* acme between MIS 14/MIS 13 and MIS 8 when this species
161 dominated (≥ 50 %) coccolithophore communities worldwide. The interval also includes the
162 extinction of *Pseudoemiliania lacunosa* in MIS 12 (Raffi et al., 2006). Neither species are found
163 in modern assemblages and their behavior cannot be assessed through cultured studies.
164 Additionally, our mid-Brunhes record precedes the first occurrence of *Emiliania huxleyi* (290 ka;
165 Raffi et al., 2006), the cosmopolitan and dominating species in the modern ocean.

166 **2. Regional setting**

167 2.1. Hydrography

168 The North Atlantic constitutes a vigorous overturning circulation of the modern ocean
169 (Toggweiler, 2009). It is characterized by the central anticyclonic subtropical gyre, the northern
170 cyclonic subpolar gyre, and continuous poleward transport of warm and salty surface waters in
171 between (Fig. 1a). This transport contributes to the Atlantic Meridional Overturning Circulation
172 (AMOC) whose strength affects regional and global climate (Rahmstorf, 2002).

173 The northern edge of the North Atlantic Current (NAC) defines the Subpolar Front,
174 which separates colder sub-arctic waters to the north from the warmer subtropical waters to the
175 south (Rossby, 1999; Priede et al., 2013). Today IODP Site U1313 is located on the southern
176 edge of the NAC. Surface waters near IODP Site U1313 are subjected to seasonal changes and
177 are influenced by eddy formation both from NAC recirculation off the Grand Banks (Fratantoni,

2001; Reverdin, 2003) and the nearby formation of the Azores Current and its associated front (Fasham et al., 1985; Schwab et al., 2012). The frontal system changes seasonally but also on geological time scales. During past glacials, fronts migrated south, reaching their southernmost limit at glacial maxima and during Heinrich events (e.g., McIntyre et al., 1972; Maslin et al., 1995, Alonso-Garcia et al., 2011).

2.2. Present productivity regime in the study area

The North Atlantic shows a distinctive latitudinal increase in primary productivity from the subtropical gyre to the north (Antoine et al., 1996a, b; Henson et al., 2009). Generally, the subpolar gyre area records the higher chlorophyll *a* concentrations with maxima during the summer months (Fig. 1b). The area characterized by transitional waters (mid-latitudes) displays intermediate levels of chlorophyll *a* concentrations (Fig. 1c), whereas the subtropical gyre exhibits lower chlorophyll *a* concentrations with maxima during winter months (Fig. 1d; note the different chlorophyll *a* scales for the respective productive regimes). *In situ* measurements, surface sediments and satellite images indicate chlorophyll and phytoplankton productivity maxima between 45º and 55º N, associated with the convergence zone between the subpolar and subtropical gyres (e.g., McIntyre et al., 1972; Weeks et al., 1993; Antoine et al., 1996a, b; Henson et al., 2009) and the meandering of the NAC (Rossby, 1999), which is characterized by higher occurrence of eddies and resultant mixing (Falkowski et al., 1991; Oschlies and Garçon, 1998; Oschlies, 2002).

Henson et al. (2009) described three areas with distinct productivity regimes in the North Atlantic. A positive correlation between chlorophyll concentration and mixed-layer depth characterizes the subtropical area, reflecting phytoplankton growth limited by nutrient availability. The subpolar area is characterized by a negative correlation reflecting light

limitation (Longhurst, 1995, 2007). IODP Site U1313 is located in the transition zone (40º to 45º N), where chlorophyll responds to changes in the mixed-layer depth and the blooms may either have subpolar or subtropical characteristics. This regime is the most variable in bloom timing and duration (Lévy, 2005; Henson et al., 2009). During summer, high SST indicates influence of subtropical, oligotrophic and stratified surface waters with a deep nutricline, resulting in low productivity. In autumn, the SST decreases and the nutricline shoals, allowing phytoplankton to bloom when sunlight is still available. Further cooling and light limitation in winter are associated with low productivity despite abundant nutrients. As soon as the duration of sunlight increases again in spring, phytoplankton (especially the opportunistic species that can grow rapidly) take advantage of the abundant nutrient availability and multiply quickly, reaching their productivity maxima during the spring bloom. At this time, the species capable of the highest growth rates, such as the coccolithophores *Emiliania huxleyi* and some species of the *Gephyrocapsa* genus, are the most abundant phytoplankton in the studied area (Broerse et al., 2000; Tyrrell and Young, 2009).

3. Material and methods

3.1. Sediment sampling and coccoliths separation

IODP Site U1313, located at 41.00º N; 32.58º W (3426 m water depth, Fig. 1), constitutes a reoccupation of Deep Sea Drilling Project (DSDP) Site 607, a reference site for Quaternary paleoceanography (Ruddiman et al., 1989; Channell et al., 2006). Four holes (U1313A to U1313D) were cored on the upper middle western flank of the Mid-Atlantic ridge, ~386 km northwest of the Azores (Fig. 1). The recovered sediment is composed of nannofossil ooze with varying amounts of foraminifers and clay- to gravel-sized terrigenous components

(Channell et al., 2006; Stein et al., 2006). For the CF Sr/Ca record a total of 409 samples were collected from ~15 meters of the secondary stratigraphic splice (15.82 to 31.15 adjusted meters composite depth (amcd) from Holes U1313A and U1313D, see Supporting Information) at 4 cm spacing using a 1 cm-wide scoop (5 cm^3). This resulted in a temporal resolution of ~700 years. Approximately 250 mg of each sample was collected and suspended in 2% ammonia to avoid carbonate dissolution, and then sieved through a 20 μm mesh to separate the coccolith fraction (<20 μm) from mostly foraminifer tests and fragments, as well as other larger microfossils and sediment components. All sieves were carefully washed with running tap water and rinsed with distilled water between samples to avoid cross contamination.

3.2. Sample preparation and Sr/Ca ratio analysis

Samples were cleaned following a three-step procedure based on Stoll and Ziveri (2002). First, 15 mL of MNX reagent (75 mg of hydroxylamine hydrochloride, 6 mL of concentrated ammonia and 9 mL of ultrapure water) was added and mixture was mechanically shaken for 12 hours. This step reduces Fe and Mn oxyhydroxides that scavenge metals from seawater and contain non-carbonate Sr. Then 2% ammonia was added to remove any non-carbonate Sr (e.g. from clays) by exchanging cations (Sr^{2+}) with the excess of NH_4^+. Finally, the mixture was rinsed with ultrapure water to extract any remaining ammonia. Initially, the procedure included a step to oxidize organic matter. However, after test results were identical with or without oxidation (Cavaleiro, 2011), possibly because of low TOC content (min=0.05 wt%; max=0.54 wt%; standard deviation=0.08 %) and high $CaCO_3$ content (min=36 wt%; max=91 wt%; mean=77 %; standard deviation=11 %), this step was removed. A weak buffered acid (6 g glacial acetic acid, 7 g ammonium acetate in 1 L of Milli-Q water) was used to dissolve the coccoliths over 12 hours to minimize the contribution of ions from non-carbonates phases. The solution was

246 then centrifuged, extracted and kept in acid-cleaned centrifuge tubes. A first inductively coupled
247 plasma-atomic emission spectroscopy (ICP-AES) measurement of Ca was performed by diluting
248 100 µL of the original sample (2 mL) into 2 mL of ultrapure Millipore water. The samples were
249 subsequently diluted to Ca concentrations similar to the standard solutions. Calibration was
250 conducted following the method described by de Villiers et al. (2002) using standards with
251 constant Ca concentrations and different Sr concentrations to give Sr/Ca ratios ranging from 0.75
252 to 4 mmol/mol. All measurements were conducted using the ICP-AES (Thermo ICAP DUO
253 6300) in the Geology Department at the University of Oviedo with reproducibility better than
254 0.02 mmol/mol. To infer any possible contamination other metals (such as Fe and Mg) were also
255 measured together with Sr.

256 3.3. Coccolith assemblage

257 As previously mentioned, the CF Sr/Ca record can be affected by changes in the
258 composition of the analyzed coccolith fraction. To investigate significant changes in the
259 coccolith assemblage, coccolith counts were performed in 24 samples selected based on their CF
260 Sr/Ca levels (8 low/ 8 intermediate/ 8 high, see Supporting Information). Samples were
261 processed following Andruleit (1996). About 0.05 g of freeze-dried sample was diluted in about
262 50 mL of buffered water, ultrasonicated for 10 s and wet-split with a rotary sample divider. One
263 one-hundredth of the solution was filtered through a polycarbonate membranes (47 mm
264 diameter, 0.4 µm pore size) with a low-pressure vacuum pump. The filters were dried in an oven
265 at 40 ºC for at least 12 hours. A randomly chosen filter area (~1 cm^2) was cut and fixed onto an
266 aluminum stub and sputtercoated with gold/palladium. At least 500 coccoliths were counted in
267 random transects using a Zeiss DMS 940A Scanning Electron Microscope at the Geosciences
268 Department, University of Bremen, using 3000× or 5000× magnification. Scanning areas varied

between 0.53 and 1.86 mm^2. Taxonomy followed *Young et al*. (2003), *Su* (1996) and Nannotax 3 (http://www.mikrotax.org/Nannotax3/index.html). Calculation of the number of coccoliths per gram of dry sediment (C) followed Andruleit (1996): C = (F * c * S) / (A * W), where F is the effective filtration area (1214 mm^2), c the number of counted coccoliths, S the split factor (1/100), A the investigated area (mm^2), and W the mass of the sample (g). To aid the visualization of contributions from different species of coccolithophores, the amount of carbonate from each of the species or species group was calculated using species-specific estimates given by Young and Ziveri (2000).

3.4. Calculation of residual CF Sr/Ca

As previously mentioned, to use the CF Sr/Ca ratio as a reliable productivity indicator, the downcore CF should not be significantly biased by variations in temperature or changes in the species assemblage composition. We therefore evaluate potential temperature effects as well as coccolith assemblage changes through time that could have affected our CF Sr/Ca ratios. Potential impacts of dissolution/preservation of coccoliths are elaborated in the Results and Discussion sections as these parameters can also be used as water-mass tracers not just influencing the CF Sr/Ca ratios.

To correct our CF Sr/Ca data for temperature changes, we use the $U^{K'}_{37}$-based SST for our site (Stein et al., 2009; Naafs et al., 2011). The alkenones in the sediment were mostly produced by coccolithophores and therefore the $U^{K'}_{37}$-based SST is the best estimate of temperature of the coccolithophores' habitat. The temperature correction of the CF Sr/Ca consisted of subtracting the SST-predicted Sr/Ca curve from the CF Sr/Ca curve:

CF Sr/Ca – SST-predicted Sr/Ca = Sr/Ca residual

To obtain the SST-predicted Sr/Ca values most representative for our record, we compare the CF Sr/Ca anomalies (Fig. 2) from three temperature dependence equations for different species or species groups and show a sensitive analysis of these anomalies on our CF Sr/Ca curve (Fig. 3).

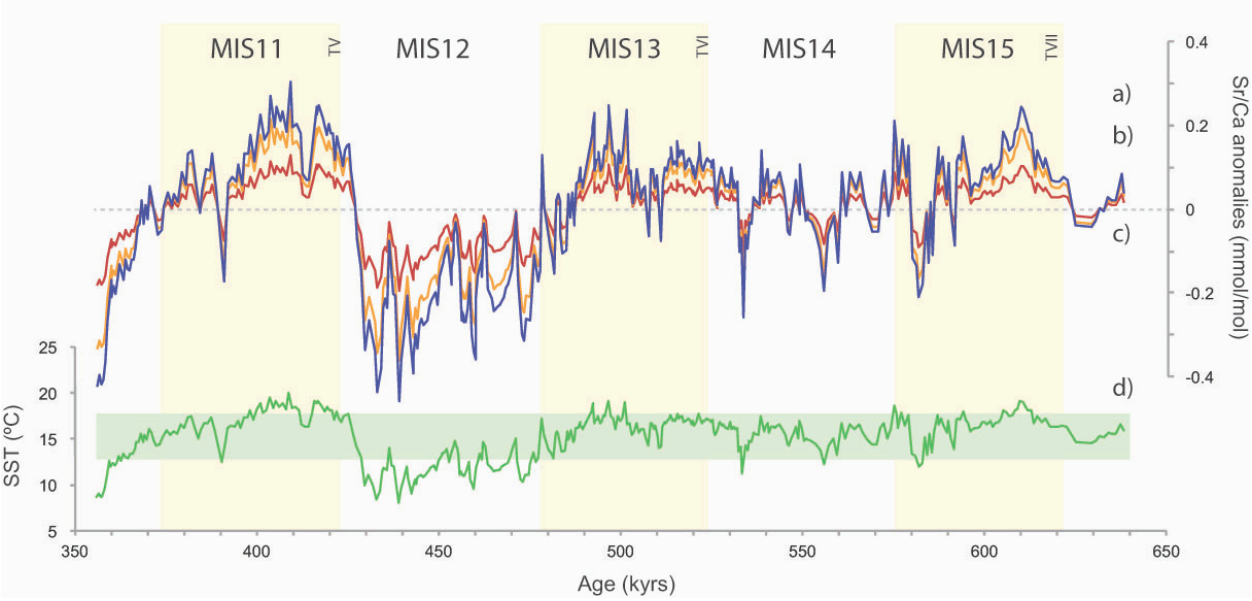

Fig. 2 - Predicted CF Sr/Ca ratio anomalies according to $U^{K'}_{37}$-SST. Each curve represent the CF Sr/Ca anomaly according to the temperature dependence of different species or group of species: a) *G. oceanica* (dark blue), b) multi-species linear regression (orange), c) *E. huxleyi* (red). The Sr/Ca deviation to negative values is a consequence of colder temperatures, while deviation to positive values reflect higher temperatures. We added the $U^{K'}_{37}$-SST record (green) for IODP Site U1313 and highlight a 5 ºC SST change to visualize that most of the SST record falls inside this range. MIS stands for Marine Isotopic Stage and each of the Terminations (T) are also identified from TV to TVII.

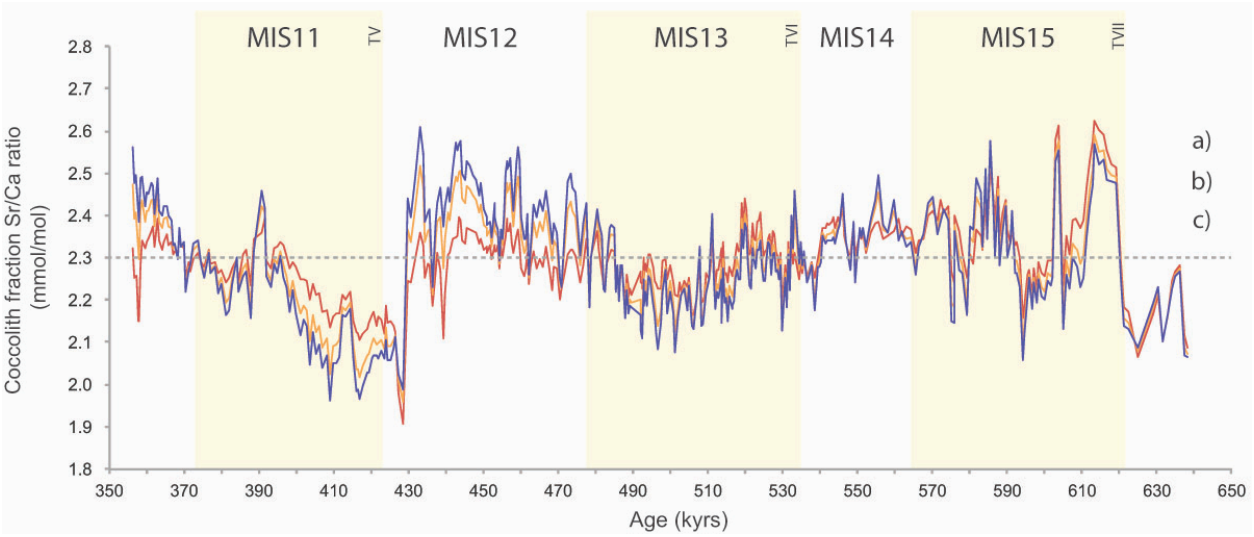

Fig. 3 - Sensitive analysis of the CF Sr/Ca anomalies caused by in SST changes on the CF Sr/Ca record. After extracting the temperature effect, each CF Sr/Ca curve shows a different amplitude according to the temperature dependence of different species or group of species: a) *G. oceanica* (dark blue), b) multi-species linear regression (orange), c) *E. huxleyi* (red). The dashed line represents the mean of the CF Sr/Ca ratio record. MIS and T as in Fig. 2.

We use the dependence of (1) *Gephyrocapsa oceanica* (Fig. 2a), a species morphologically similar to *Gephyrocapsa caribbeanica* that dominates our sediments, and compare it with (2) a multi-species dependence that combines *G. oceanica*, *Calcidiscus leptoporus*, *Helicosphaera carteri* and *Coccolithus pelagicus* (Fig. 2b). Finally, the dependence of (3) *Emiliania huxleyi* is also shown (Fig. 2c) on the rationale that this species and *G. caribbeanica* share a cosmopolitan and dominant presence in deep-sea sediments, albeit at different times. Whereas *E. huxleyi* rose to dominance at ~80 ka (*Raffi et al.*, 2006) and is still extant, *G. caribbeanica* had a similar distribution and dominance during the Mid-Brunhes interval (*Bollmann et al.*, 1998). The three respective equations are shown here:

(1) $y = (0.0636*x) + 1.3944$ (Stoll et al., 2002b)

(2) $y= (0.0501*x) + 1.7053$ (Mejía et al., 2014)

(3) $y = (0.0272*x) + 2.4238$ (Stoll et al., 2002b)

where y is the predicted coccolith Sr/Ca value according to a given temperature x.

Anomalies based on *G. oceanica* (Fig. 2a) and the multi-species group (Fig. 2b) are similar, as are the CF Sr/Ca ratios of the sensitivity analysis (Fig. 3a and b). To decide which equation to use, we looked at the coccolith assemblage changes. Although the continuous presence of *G. oceanica* in our sediments and its similarities to *G. caribbeanica* favor the use of its temperature dependence (1), the beginning of our record contains a substantial number of non-gephyrocapsids (Fig. 4). From MIS 14 to MIS 10, our sedimentary record is dominated by *G. caribbeanica*, which constitutes 50 to 80 % of the assemblage (Fig. 4a). The assemblages from late MIS 16 until mid MIS 14 contain, however, higher abundances of larger and more heavily calcified coccoliths, such as *Calcidiscus leptoporus and Helicosphaera carteri*. This becomes even clearer when the numbers of coccoliths are converted into species-specific contribution to the $CaCO_3$ content (Young and Ziveri, 2000) (Fig. 4b).

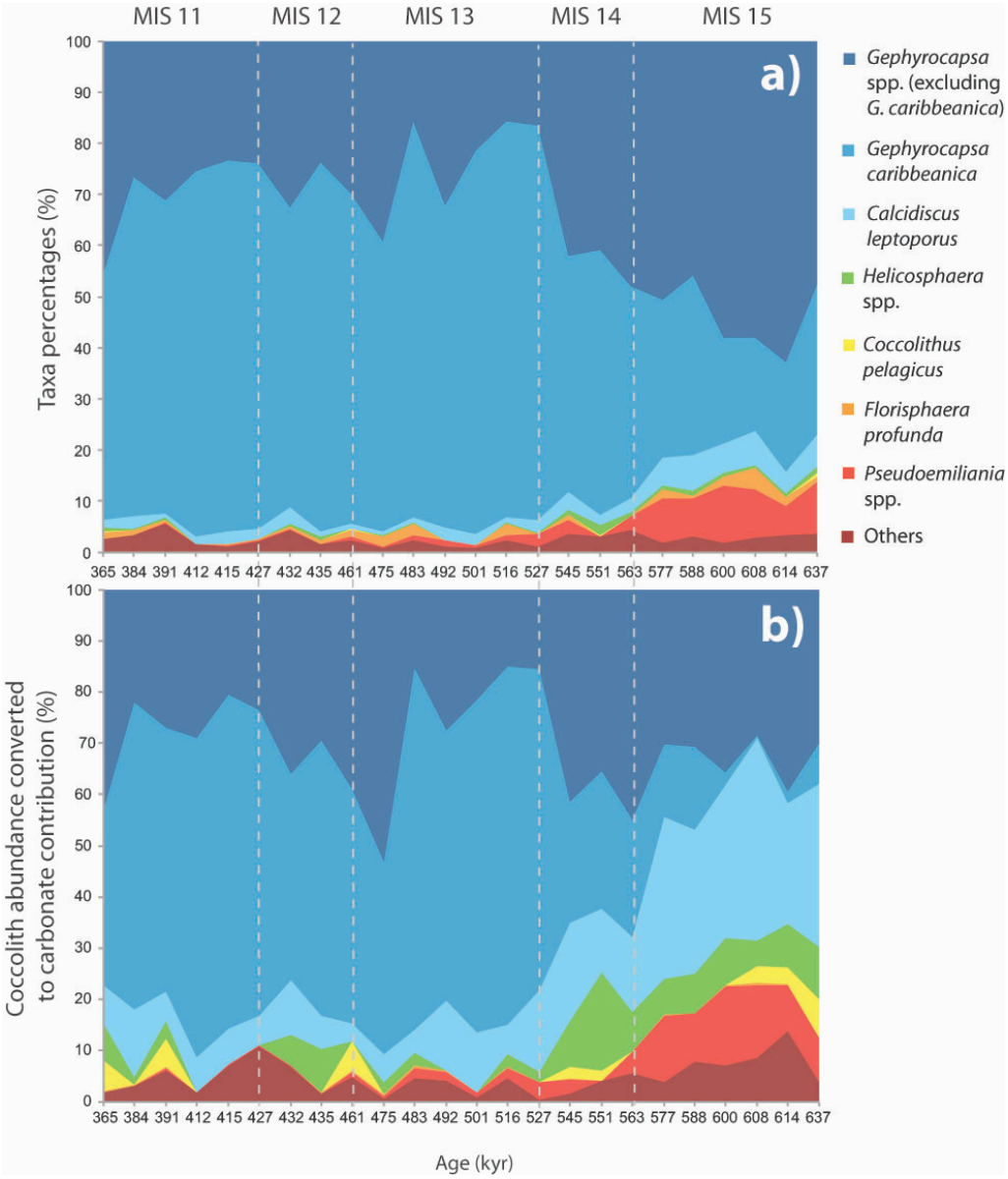

Fig. 4 - Coccolith assemblage results: a) coccolith relative abundance (%); b) coccolith abundance converted to relative carbonate contribution (%). Please note that the samples are not evenly spaced in time.

Based on these observations and the absence of *E. huxleyi* in our sediments, we rejected the species-specific curves and use the Sr/Ca residual resultant from the multi-species temperature dependence (Fig. 5a). We refer to this residual from here on as coccolithophore productivity, because after correcting for temperature changes, we expect the curve to mostly reflect coccolithophore growth rate and thus paleoproductivity variations. The coccolithophore

339 productivity record reflects relative productivity change, representing the productivity deviation
340 around the average productivity of the time series.

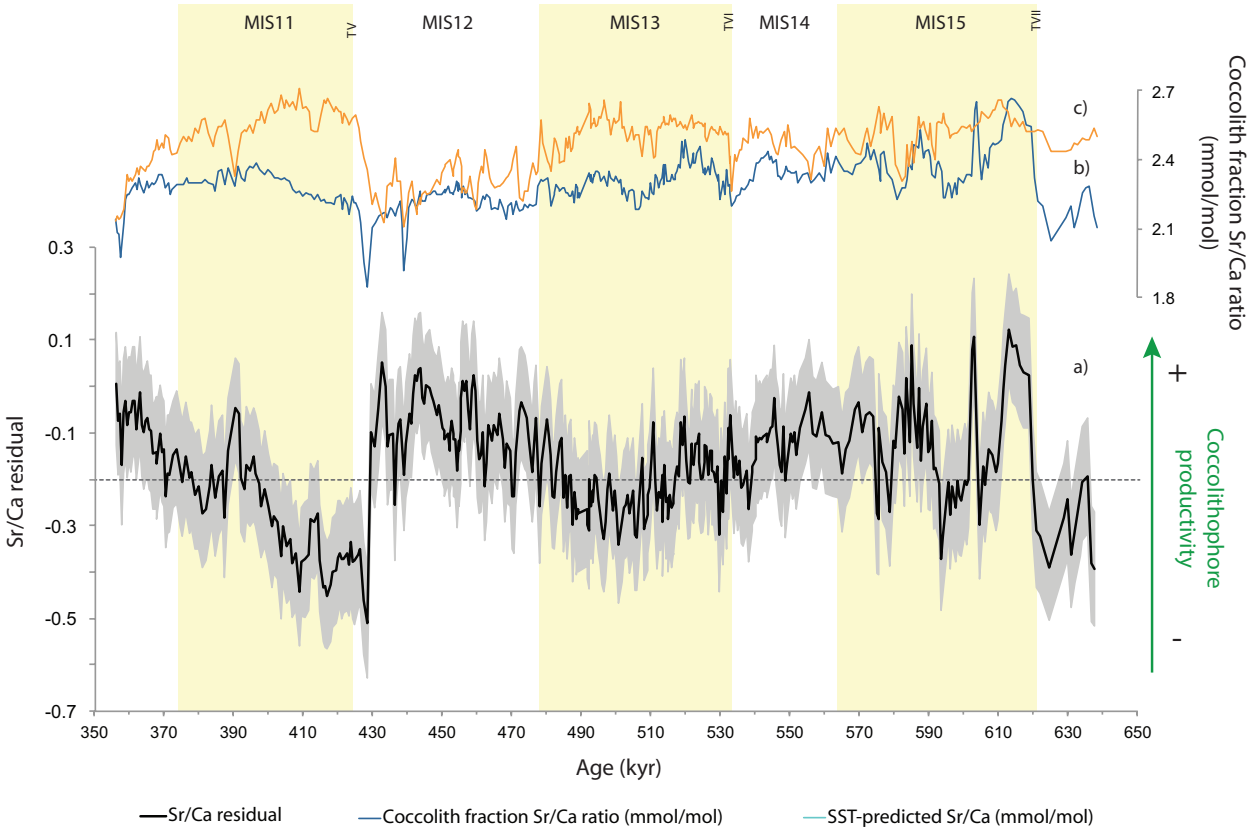

341

342 Fig. 5 - Sr/Ca results: a) CF Sr/Ca residual record (black curve) with confidence interval (grey area; Monte Carlo 20 to 80%
343 interval), b) coccolith fraction Sr/Ca results (dark blue curve), and c) SST-predicted Sr/Ca ratio curve (orange curve). The CF
344 Sr/Ca residual curve corresponds to the reconstructed coccolithophore productivity with the dashed line indicating the mean:
345 values above the mean represent higher coccolithophore productivity and below the mean lower coccolithophore productivity.
346 MIS and T as in Fig. 2.

347 Finally, to accommodate for potential biases caused by short intervals of large amplitude
348 SST changes not present in previous studies, we determined an uncertainty envelope/confidence
349 interval (shown as a grey envelope in figures) for the CF Sr/Ca residual. Using Astrochron
350 (Meyers, 2014) we ran 100 Monte Carlo simulations for each of the 409 data points and carried
351 out propagation of errors accounting for measurement uncertainties of temperature (with σ =

352 1.5°C) and Sr concentration (with σ = 0.01 mmol/mol), and the linear regression of temperature
353 versus Sr (σ = 0.12 mmol/mol). All figures showing the paleoproductivity record are
354 accompanied with a grey envelope whose upper and lower limits correspond to Monte Carlo 20
355 and 80 % confidence intervals (following Mejía et al., 2014).

356 3.5. Additional proxy data

357 The residual Sr/Ca curve is compared to carbonate content, carbon and oxygen isotopes
358 and coccolith assemblages and preservation data to infer the likelihood and severity of
359 dissolution. A coccolith dissolution index (CDI) based on the differential dissolution behavior of
360 different coccoliths was adapted from Dittert et al. (1999) to estimate the effect of carbonate
361 dissolution on the coccolith assemblages. We calculate the ratio between small *Gephyrocapsa*,
362 which are relatively fragile and more susceptible to dissolution, and *Calcidiscus leptoporus*, a
363 larger and more robust placolith. We used small *Gephyrocapsa* because *E. huxleyi* (suggested as
364 the fragile placolith by Dittert et al. (1999)) is not present in our sediments. The CDI is
365 calculated as follows: CDI = (small *Gephyrocapsa* (%)) / (small *Gephyrocapsa* (%) +
366 *Calcidiscus leptoporus* (%)).

367 The $U^{K'}_{37}$-based SST record for Site U1313 is already published (Stein et al., 2009; Naafs
368 et al., 2011), whereas some of the TOC and total alkenone concentration data are being published
369 here for the first time. Methods for TOC and alkenone concentration analysis and methodology
370 are described in Stein et al. (2009).

371 The methods used to generate the benthic foraminifer stable isotope data is presented in
372 Voelker et al. (2010), whereas calculation of the polar planktonic foraminifer *Neogloboquadrina*
373 *pachyderma* (formerly *N. pachyderma* (s)) percent in the fraction >150μm fraction follows

374 standard micropaleontological procedure (e.g., Voelker et al., 2009). Sediment carbonate content
375 was estimated from the X-ray fluorescence (XRF) Ca data (see Grützner and Higgins (2010) for
376 details on XRF measurements). The Ca intensity counts obtained by XRF scanning were
377 calibrated through correlation ($r^2 = 0.84$) with 517 quantitative carbonate analyses on discrete
378 samples (Stein et al., 2009) using a power function.

379 3.6. Age model

380 Voelker et al. (2010) constructed the age model for Site U1313 by correlating the benthic
381 foraminifer oxygen isotope record ($\delta^{18}O_b$) with the LR04 stack (Lisiecki and Raymo, 2005) with
382 most correlation points being isotopic maxima (Fig. S1). Both $\delta^{18}O_b$ and CF Sr/Ca were
383 measured in samples from the secondary splice (Holes U1313A and U1313D), whereas the $U^{K'}_{37}$-
384 based SST data, used to correct the CF Sr/Ca initial curve, were obtained from primary splice
385 samples (Holes U1313 B and U1313C). We used linear interpolation to match the resolution of
386 the CF Sr/Ca record. Both alkenone and TOC samples were collected from the primary splice, at
387 2 cm spacing. Using data from both splices was possible because the lightness (L*) records of
388 the four holes (U1313A to U1313D) were visually correlated to create a common adjusted meter
389 composite depth (amcd) (Naafs et al., 2012). Using the amcd depths, the age model of Voelker et
390 al. (2010) could then be applied to both the primary and secondary splice.

391 3.7. Time-series analysis

392 Spectral analysis was conducted to test for statistically significant periodicities in the
393 coccolithophore productivity record. The harmonic analysis of SPECTRUM was used to filter
394 the time series for specific frequencies (see Supporting Information). Because the CF Sr/Ca
395 (coccolithophore productivity) record is an unevenly spaced time series (i.e., the time between

396 samples varies), we decided to use the SPECTRUM and REDFIT packages for the time series
397 analysis (Schulz and Stattegger, 1997; Schulz and Mudelsee, 2002), the only packages able to
398 execute time series analysis without interpolation of the real data to produce an evenly spaced
399 time series. A band-pass filtered Gaussian curve of the coccolithophore productivity record was
400 computed with the Analyseries software package (Paillard et al., 1996) to allow visual alignment
401 with the monthly insolation curves for the same time period. To test the hypothesis of changing
402 coccolithophore phenology through time, we used time series analysis to look for orbital and
403 suborbital periodicities in the coccolithophore productivity record (see Supporting Information).

404 **4. Results**

405 4.1. CF Sr/Ca results and other productivity proxies

406 The CF Sr/Ca values range from 1.85 to 2.67 mmol/mol (Fig. 5b), with 85% of the data
407 within the range of 2.1 to 2.5 mmol/mol. This represents 49% of the whole sampling variation,
408 with a total sampling range of 0.82 mmol/mol. The CF Sr/Ca values vary between ± 10% with an
409 average variation of 1.6%. Higher variability is present in the beginning of the record (MIS 16
410 and MIS 15) with distinct minima at 439, 428 and 427 ka (MIS 12), while maxima values are
411 found at 613, 603 and 587 ka (during MIS 15). The Sr/Ca residual data, referred to as the
412 coccolithophore productivity record, show maxima coincident with the CF Sr/Ca record during
413 MIS 15, several intermediate peaks during MIS 14, maxima similar to those found in MIS 15
414 during MIS 12 (at 457, 443 and 433 ka) and slightly lower values in early MIS10 (390 kyr).
415 Minima occurred in late MIS 16 (625 ka), during MIS 15 (605 and 594 ka), around Termination
416 (T) V (428 ka), and during MIS 11 (416 and 408 ka).

417 Both the CF Sr/Ca ratios and coccolithophore productivity record reveal an abrupt
418 increase from MIS 16 to MIS 15 and a general decreasing trend from early MIS 15 to late MIS
419 13 (~610 ka until ~490 ka), although with higher amplitude variability in MIS 16 and MIS 15
420 than within the rest of the record (Fig. 5). From mid-MIS 13 until TV the records show opposite
421 trends: coccolithophore productivity increases, whereas the CF Sr/Ca shows a decreasing trend.
422 TV marks a very abrupt change in coccolithophore productivity, from high values to the lowest
423 of the record. From that point to the end of the record in MIS10, coccolithophore productivity
424 increases. Noteworthy are the higher CF Sr/Ca rations in MIS 12 (from ~470 to 440 ka) relative
425 to those in the MIS 11 interglacial period (from TV until ~400 ka), despite the lower SST (~13
426 ºC in MIS 12 compared to ~18 ºC during interglacial MIS 11).

427 The glacial-interglacial pacing of the coccolithophore productivity record is usually
428 characterized by an increase during glaciation, with higher variability and amplitude than during
429 interglacial. Maxima occur in MIS 12 and, exceptionally, the beginning of MIS 15. Glacial MIS
430 14 and MIS 12 show higher average values in comparison with interglacial MIS 15, MIS 13 and
431 MIS 11. Abrupt decreases occur found at TVI and TV, even though the amplitude of TVI is less
432 than half that of TV. Lower values are found in MIS 15 and MIS 11 interglacials (Fig. 5a).
433 Coccolithophore productivity thus shows variability at both orbital and suborbital time scales
434 with generally higher values during glacials (except during late MIS 16) and lower values during
435 interglacials.

436 The TOC and total alkenones concentration records (Fig. 6a and b) reveal similar
437 patterns, with low values and low amplitude oscillations in MIS 15, MIS 13 and MIS 9
438 contrasting with higher levels and higher amplitude oscillations in MIS 16, MIS 14 and MIS 12.
439 The $CaCO_3$ content (Fig. 6c) records lower values in MIS 16 (including a minimum of almost 30

440 %) and a steady and rapid increase at TVII. High values and a slight increasing trend are present
441 from TVII to the beginning of MIS 12. The $CaCO_3$ content decreases steadily in MIS 12, with
442 large oscillations and several decreases to almost 50 %.

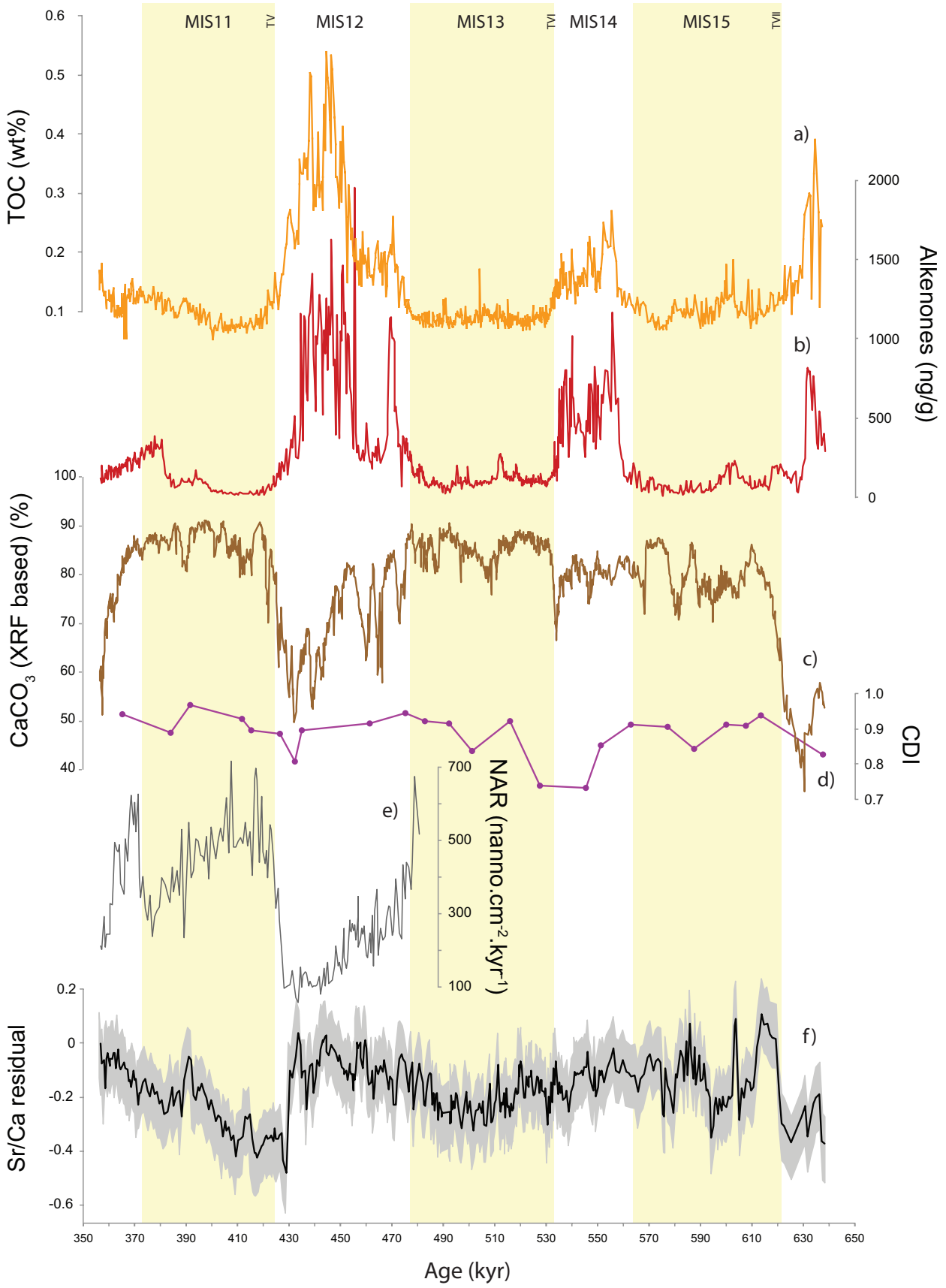
MIS11
TV
MIS12
MIS13
TVI
MIS14
MIS15
TVII
TOC (wt%)
0.6
0.5
0.4
0.3
0.2
0.1
a)
2000
1500
1000
500
0
Alkenones (ng/g)
b)
100
90
80
70
60
50
40
CaCO3 (XRF based) (%)
c)
1.0
0.9
0.8
0.7
CDI
d)
e)
700
500
300
100
NAR (nanno.cm-2.kyr-1)
0.2
0
-0.2
-0.4
-0.6
Sr/Ca residual
f)
350
370
390
410
430
450
470
490
510
530
550
570
590
610
630
650
Age (kyr)

443

444 Fig. 6 - Primary productivity proxies: a) total organic carbon (TOC) weight % (Stein et al., 2009; this study), , b), total alkenones
445 concentration (ng/g of sediment) (Stein et al., 2009; this study) c) calcium carbonate ($CaCO_3$) content based on XRF
446 measurements (this study), d) Coccolith Dissolution Index (CDI) (this study): the closest to 1, the lower the likelihood of
447 dissolution/ the better the preservation, e) nannofossil accumulation rate (NAR) (nannofossils·cm^{-2}·kyr^{-1}) (Kulhanek, 2009), f)
448 reconstructed coccolithophore productivity (and confidence interval) based on coccolith Sr/Ca ratios (this study). MIS and T as in
449 Fig. 2.

450 ## 4.2. Coccolith preservation and dissolution

451 Coccolith preservation is moderate to good in MIS 12 to MIS 10 (Kulhanek, 2009) and
452 the calculated CDI indicates good preservation throughout the examined record to MIS 16 (Fig.
453 6d). CDI shows no correlation with the CF Sr/Ca or residual record, even in MIS 12, when
454 corrosive southern sourced waters invaded the deep glacial North Atlantic (Thunell et al., 2002;
455 Voelker et al., 2010) as suggested by the lower benthic carbon isotopic values at Site U1313 in
456 MIS 12 and MIS 16 (Fig. 7a).

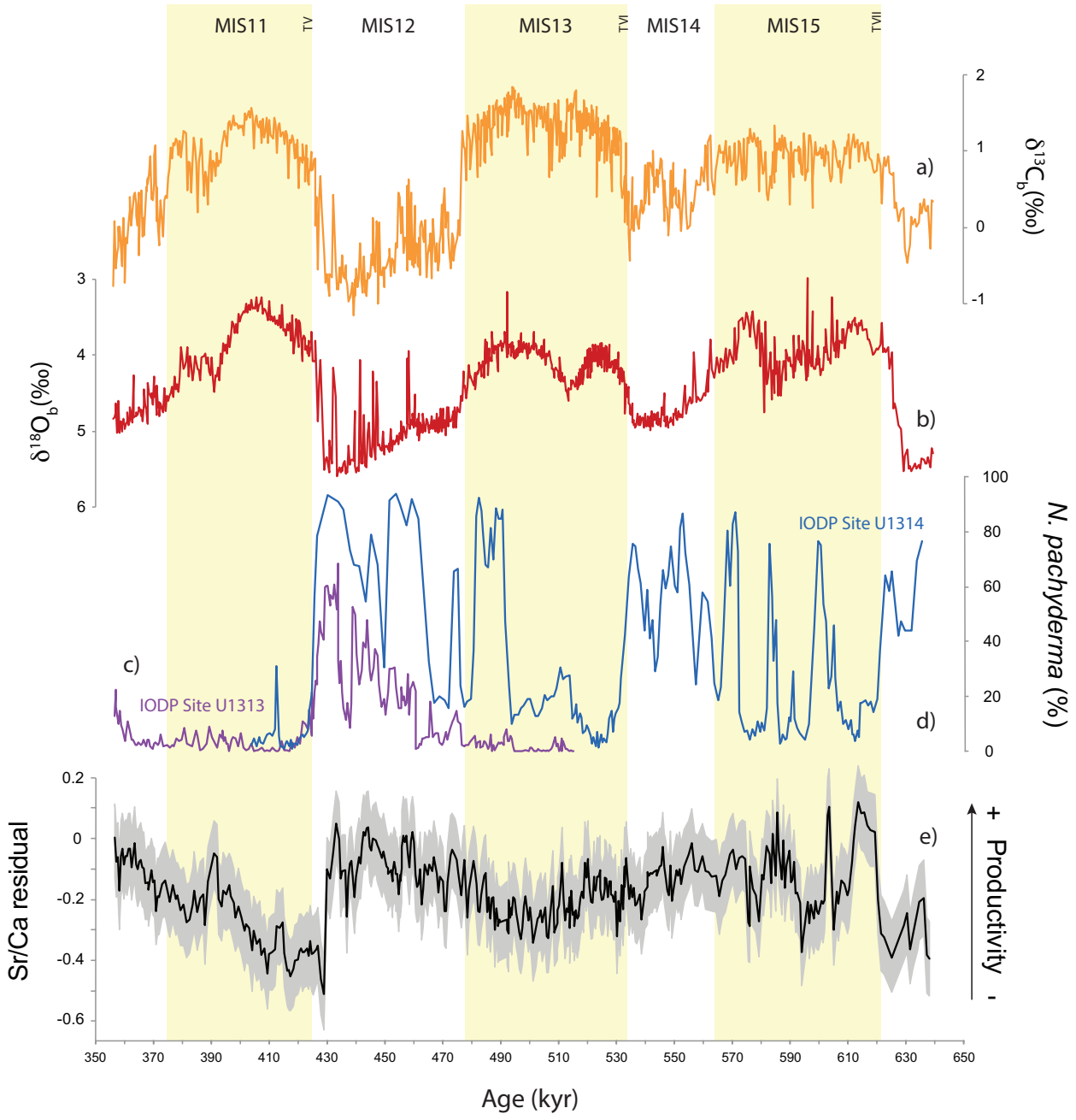

Fig. 7 - Ventilation and water mass time series: a) benthic foraminifera carbon isotope data ($\delta^{13}C_b$) (Voelker et al., 2010 and this study), b) benthic foraminifera oxygen isotope data ($\delta^{18}O_b$) (Stein et al., 2009; Voelker et al., 2010), c) and d) correspond to the relative abundance of *N. pachyderma* at IODP Site U1313 (this study) and IODP Site U1314 (Alonso-Garcia et al., 2011), respectively, e) reconstructed coccolithophore productivity (and confidence interval) based on coccolith Sr/Ca ratios (this study). MIS and T as in Fig. 2.

463 4.3. Time-series analysis

464 We applied spectral analysis to look for statistically significant periodicities in the
465 coccolithophore productivity record and found a robust precessional signal and two additional
466 significant periodicities that are ~15 kyr for the CF Sr/Ca record (Fig. 8a) and ~9 kyr for
467 coccolithophore productivity (Fig. 8b). The two significant periodicities, ~15 kyr and ~9 kyr, are
468 consistently found despite applying different filtering and smoothing methodologies, which gives
469 robustness to our findings (see Supporting Information). The periodicities detected in the
470 coccolithophore productivity time series are not observed in the $U^{K'}_{37}$-based SST record (Fig. 8c),
471 whereas the total alkenone concentration record exhibits periodicities close to 9 kyr but with
472 lower significance (see Supporting Information). Additionally, all methodologies consistently
473 reveal a small but significant peak at 2.6 kyr. This cyclicity has been found in other North
474 Atlantic time series (e.g., Pisias et al., 1973). However, since it is near the lower detection limit
475 (sample resolution is 700 years) and below the age model uncertainties (4 kyr), (Lisiecki and
476 Raymo, 2005)), it is not discussed further.

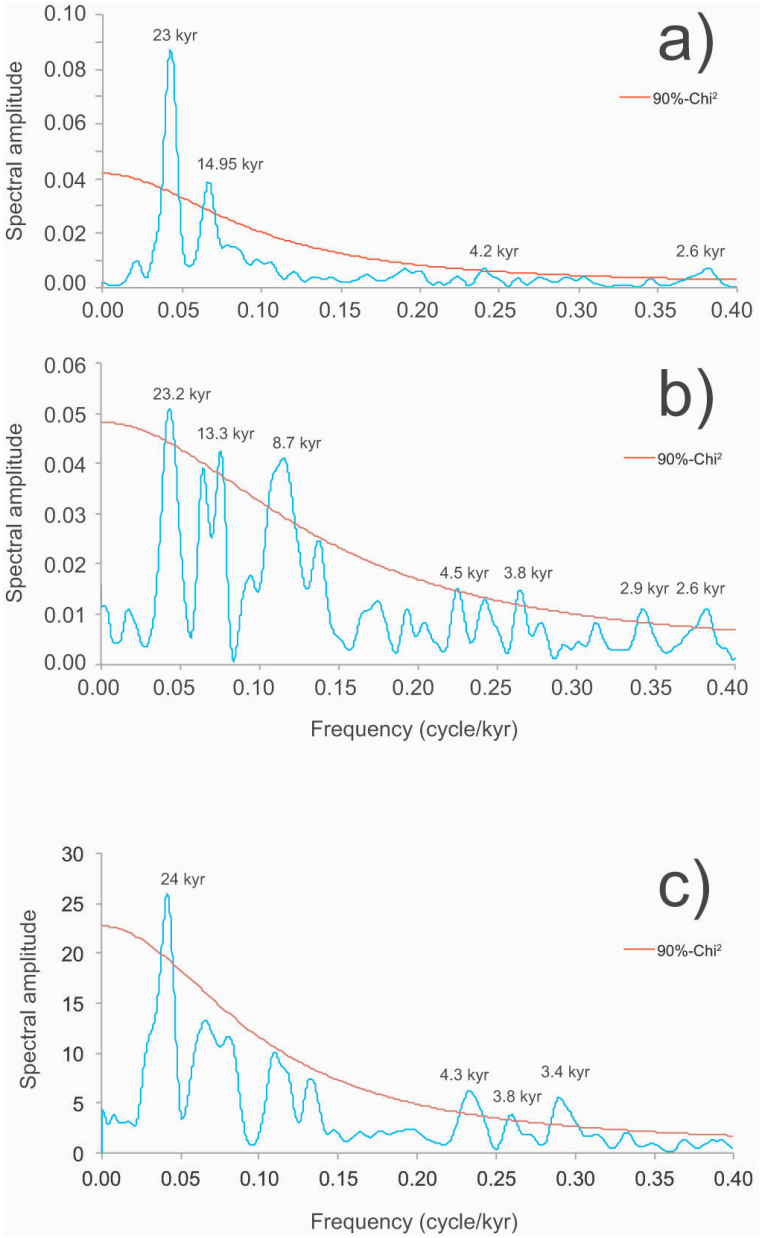

Fig. 8 - Spectral power results in REDFIT: (a) for the coccolith Sr/Ca ratio time series and (b) for the coccolithophore productivity record. We also present the spectral power results for the $U^{K'}_{37}$-SST (c), for comparison. All records were filtered in SPECTRUM to extract significant frequencies above 1/40kyr and 1/23 kyr, respectively. Bandwidth for all spectral power results is 1.12×10^{-2}. The red lines represent the significance level of 90% Chi^2 (peaks below this line correspondent to periodicities which are not significant).

5. Discussion

5.1. Coccolithophore productivity record

Culture studies have found that coccolith Sr/Ca may increase by 0.03 mmol/mol per ºC rise in temperature (Stoll et al., 2002a; Müller et al., 2014). Given the modest variation of the CF Sr/Ca ratios for most of our record (Fig. 5b) and the consistent temperature variations in the range of 5 ºC, the temperature-induced Sr/Ca variation could be about 0.15 mmol/mol. Moreover, during TV, temperature rose by almost 10 ºC. Therefore, SST must be considered as a potential contributor to the CF Sr/Ca ratios. We removed the temperature effect (see 3.4 Calculation of residual Sr/Ca) and the resulting curve, the Sr/Ca residual (Fig. 5c), reveals a persistent temporal pattern not evident in the CF Sr/Ca ratios that we interpret to be dominated by coccolithophore calcification/growth rate and thus paleoproductivity.

Changes in the coccolithophore assemblage may also have an effect on the CF Sr/Ca. In our record there is a change in dominance from larger, more calcified species in MIS 16 – MIS 15 to abundant *Gephyrocapsa caribbeanica* in the rest of the record. However, coccolith assemblage appears to exert a minor influence on CF Sr/Ca in the modern ocean (Stoll and Schrag, 2000) and the specific coccolith carbonate estimations, shown in Fig. 4b, have inevitable but substantial errors associated (±50%) (Young and Ziveri, 2000). It seems thus unlikely that the coccolith assemblage changes affected significantly our proxy, but to address the possibility of the existence of a caveat (if any) the coccolithophore productivity record for MIS 16 – MIS 15 should be interpreted more carefully and regarded as a conservative estimate of coccolithophore productivity. Noteworthy is the fact that the *Gephyrocapsa caribbeanica* acme spans the studied interval and constitutes an advantage as it minimizes the CF Sr/Ca ratio bias due to coccolith assemblage changes.

5.2. Effect of the southernmost position of the frontal system on coccolithophore productivity at Site U1313

The positions of ocean frontal systems around Site U1313 change not only seasonally, but also throughout geological time. During glaciations, the North Atlantic Polar and Arctic/subpolar Fronts migrated southward and several authors have suggested an almost east-west position of the Arctic Front (Wright and Flower, 2002; Alonso-Garcia et al. 2011; Rodrigues et al., 2017). The high coccolithophorid productivity belt also migrated southward (McIntyre et al., 1972; Villanueva et al., 2001) in pace with changes in the positions of these hydrographic fronts. This belt, currently located between 45º and 55º N, is associated with the convergence zone between the subpolar and subtropical gyres (Weeks et al., 1993), and may have moved as far south as 42º N during glacials (McIntyre et al., 1972; Villanueva et al., 2001).

These large migrations of the frontal systems and high productivity band likely impacted Site U1313 during glacials. During the most severe glacials, evidenced by the highest benthic oxygen isotopic values in the record (e.g., MIS 12; Fig. 7b), or the Heinrich events, Site U1313 might have seasonally shifted into the subpolar region, outside of the coccolithophore habitat.

If subpolar/polar surface waters reached Site U1313 during glacial periods, the extremely low temperatures could lead to the reduction or disappearance of the coccolithophore community due to loss of habitat (McIntyre et al., 1972). Today, coccoliths in surface sediments of the Norwegian-Greenland Sea (i.e. in the polar domain) are mainly restricted to areas beneath subpolar surface waters, whereas very low coccolith concentrations are found in sediments underlying the sea-ice covered Arctic and polar waters (Baumann et al., 2000). To test whether subpolar/polar surface waters reached our study site we use the percentage *N. pachyderma* record (Fig. 7c). *N. pachyderma* is the most abundant planktonic foraminifer species in polar

530 (perennially covered by sea ice) and Arctic (seasonally ice covered) waters (Johannessen et al.,
531 1994; Kucera et al., 2005; Alonso-Garcia et al., 2011). Today, relative abundances of *N.*
532 *pachyderma* higher than 65% are indicative of the Arctic Front (Johannessen et al., 1994), which
533 separates Arctic surface waters from the subpolar surface waters. Except for one instance with
534 68% *N. pachyderma* at 433 ka (MIS 12), the relative abundance of *N. pachyderma* is lower than
535 65% at Site U1313. If we compare the relative abundance of *N. pachyderma* at Site U1313 (our
536 study; Fig. 7c) to Site U1314 (Alonso-Garcia et al., 2011; Fig. 7d), located at 56º N, the northern
537 site was under greater influence of Arctic and even polar waters for longer periods than Site
538 U1313. Based on these observations, we conclude that the coccolithophore community was not
539 heavily affected by the loss of habitat during the studied time period because the Arctic front did
540 not reach as far south as Site U1313 (41º N), at least not within the temporal resolution of this
541 study. However, there were periods when subpolar surface waters (% *N. pachyderma* ≥ 20%)
542 influenced Site U1313.

543 5.3. Drivers of coccolithophore productivity

544 All phytoplankton productivity is controlled by a combination of variables, of which light
545 intensity and nutrient availability are considered the most relevant (Barbosa, 2009). We
546 investigated these controlling factors focusing first on the hydrographical changes affecting
547 coccolithophore productivity at our study site.

548 5.3.1. Nutrient supply

549 Coccolithophore productivity is linked to nutrient availability (Brand, 1994; Balch, 2004;
550 Marinov et al., 2010; Müller et al., 2017), which in the open ocean reflects circulation (Herbert
551 and Sarmiento, 1991). Therefore, we first hypothesized that the observed periods of high

552 coccolithophore productivity in our record reflect changes in regional hydrography that increased
553 nutrient availability. This process could indeed explain the glacial – interglacial productivity
554 pattern. In this scenario, the North Atlantic atmospheric and oceanic frontal systems shifted
555 southward during cold periods (e.g., Alonso-Garcia et al., 2011; Frank et al., 2011) and, as
556 proposed by McIntyre et al. (1972), the nutrient-driven "high productivity band", also shifted
557 southward. Villanueva et al. (2001) examined productivity based on alkenone content at two
558 North Atlantic sites located at 37º N and 43º N (Fig. 1). They explained the time discrepancy in
559 several of the productivity events as a consequence of this high productivity band migration.
560 This is consistent with our findings that suggest that Site U1313 (41º N) was under the influence
561 of this "high productivity band" during glacials, enhancing coccolithophore productivity.

562 Dust delivery has also been suggested as a fertilization mechanism for oceanic
563 productivity (e.g., Martin et al., 1990). Naafs et al. (2012) reconstructed aeolian input at Site
564 U1313 based on the concentrations of long-chain n-alkanes and terrestrial plant waxes, which
565 indicate increased North American dust input during cold periods as a consequence of the
566 waxing and waning of continental ice sheets and increased westerly wind strength. Stronger
567 winds over the surface ocean during colder periods could also increase mixing depth (Barton et
568 al., 2003), enhancing nutrient replenishment to the surface.

569 In addition to the dominant pattern of higher productivity during glacials, our
570 coccolithophore productivity record indicates substantial variability at higher frequencies (Fig.
571 8). Thus, despite the effect of frontal migrations, there must have been other processes, such as
572 changes in insolation, modulating coccolithophore productivity at the studied site.

573 5.3.2. Insolation

574 Insolation intensity, which changes cyclically through geological time, is a result of the
575 combined changes in Earth's orbital parameters (eccentricity, obliquity and precession) (e.g.,
576 Berger, 1988; Laskar et al., 2004). It directly influences the amount of light and temperature
577 conditions at the surface of the ocean, which in turn affect organisms behavior (Vallina and
578 Simó, 2007). Since both light and temperature enhance photosynthesis, the modulation of
579 insolation could affect coccolithophore productivity. This could be a direct effect or it could act
580 by modulating the phenology of the phytoplankton at the studied site. Coccolithophores require
581 light to photosynthesize. Therefore, increases in insolation should enhance coccolithophore
582 productivity (Nimer and Merrett, 1993; Zhang, 2015).

583 Site U1313 is currently located in a transitional area (Fig. 1a) with a mid-latitude
584 productivity regime generally characterized by two productivity peaks per year, one in spring
585 and the other in autumn (Fig. 1c) (Lévy, 2005). If coccolithophores living in this area were to
586 experience higher productivity in spring and autumn (6 months apart) throughout the
587 Pleistocene, these higher production periods would have coincided with insolation peaks for
588 those two seasons. As a result, we would expect the record to show a precessional (~23 kyr) and
589 semi-precessional (~11.5 kyr) enhancement of productivity would be expected in the
590 productivity record (Fig. 9a and b). However, in addition to the precessional signal, the
591 coccolithophore productivity record contains significant periodicities at "unusual" frequencies of
592 ~15 kyr and ~9 kyr (Fig. 8).

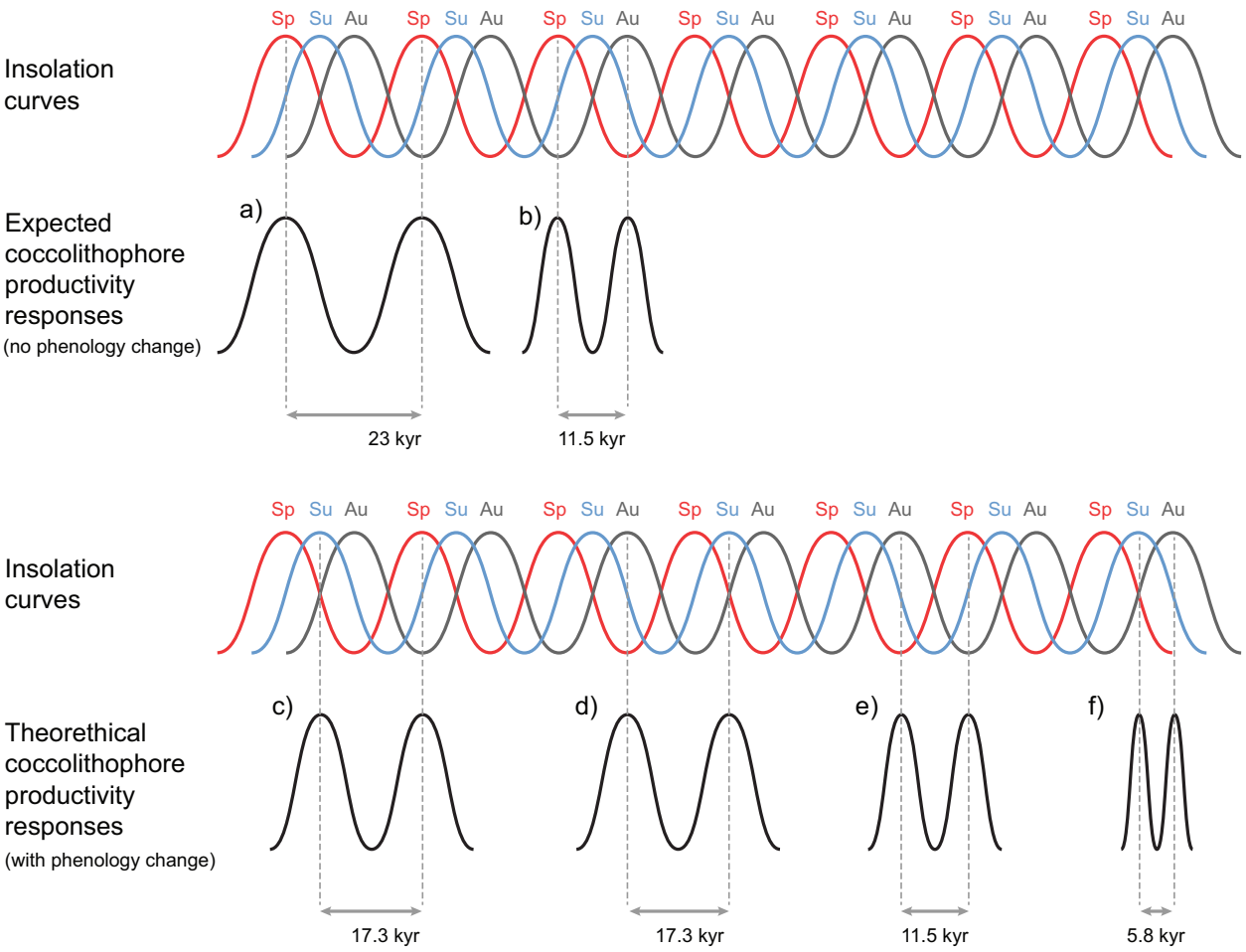

Fig. 9 - Theoretical coccolithophore community response to insolation forcing. Expected theoretical cyclicity for coccolithophore productivity: a) precessional (23 kyr), b) semi-precessional (11.5 kyr). Theoretical cyclicity found for coccolithophore productivity: c and f) 17.3 kyr, f) 11.5 kyr) or g) 5.8 kyr. Season abbreviations: Sp = spring, Su = summer, Au = autumn. Each sine wave represents a theoretical curve of insolation for each season: red corresponds to spring, blue to summer and grey to autumn.

We then examine whether these periodicities could be an artifact of the age model. The age model was based on visual correlation of the Site U1313 benthic oxygen isotope record (Voelker et al., 2010) with the LR04 stack (Lisiecki and Raymo, 2005). The resolution of the benthic oxygen isotope record is higher than our coccolithophore productivity record and because both records are from the same archive, the age model should be free of artifacts due to

phase shifts or resolution. Due to the lag in propagation of the oxygen isotope signal throughout the ocean, this age model contains an uncertainty of about 4 kyr (Lisiecki and Raymo, 2005), but the dating of glacial cycles is robust and the uncertainty is less when considering durations. Therefore, the inferred duration of our record (~310 kyr) is relatively robust. If the observed productivity peaks in the high-frequency part of the spectrum reflect semi-precession, we should observe about 30 such peaks throughout the record. However, we find 22 productivity peaks (Fig. 10), implying that the identified periodicities cannot be reconciled with semi-precessional forcing.

The $U^{K'}_{37}$-based SST and the total alkenone concentration record do not reveal a 15 kyr periodicity (Fig. 8c and Supporting Information). This unusual frequency is thus exclusive to the coccolithophore productivity record. There is some evidence for similar high-frequency variability in the TOC and total alkenone data (Fig. 6a and b), but this is only manifested during glacials. During interglacials, both TOC and alkenone concentration are low and reflect poor preservation of organic matter in the sediments, precluding a meaningful spectral analysis of the records. Since there is no evidence for migration of the frontal systems around the studied site at these high frequencies especially during the interglacials, we instead look at insolation forcing. To better visualize these periodic components in the coccolithophore productivity, the record was filtered at a 14 kyr band pass with a 20 kyr bandwidth to produce a Gaussian smoothed curve (pink line in Fig. 10e). This facilitated a visual inspection of the position of the individual productivity peaks with respect to monthly insolation (Laskar et al., 2004) over the studied interval (Fig. 10).

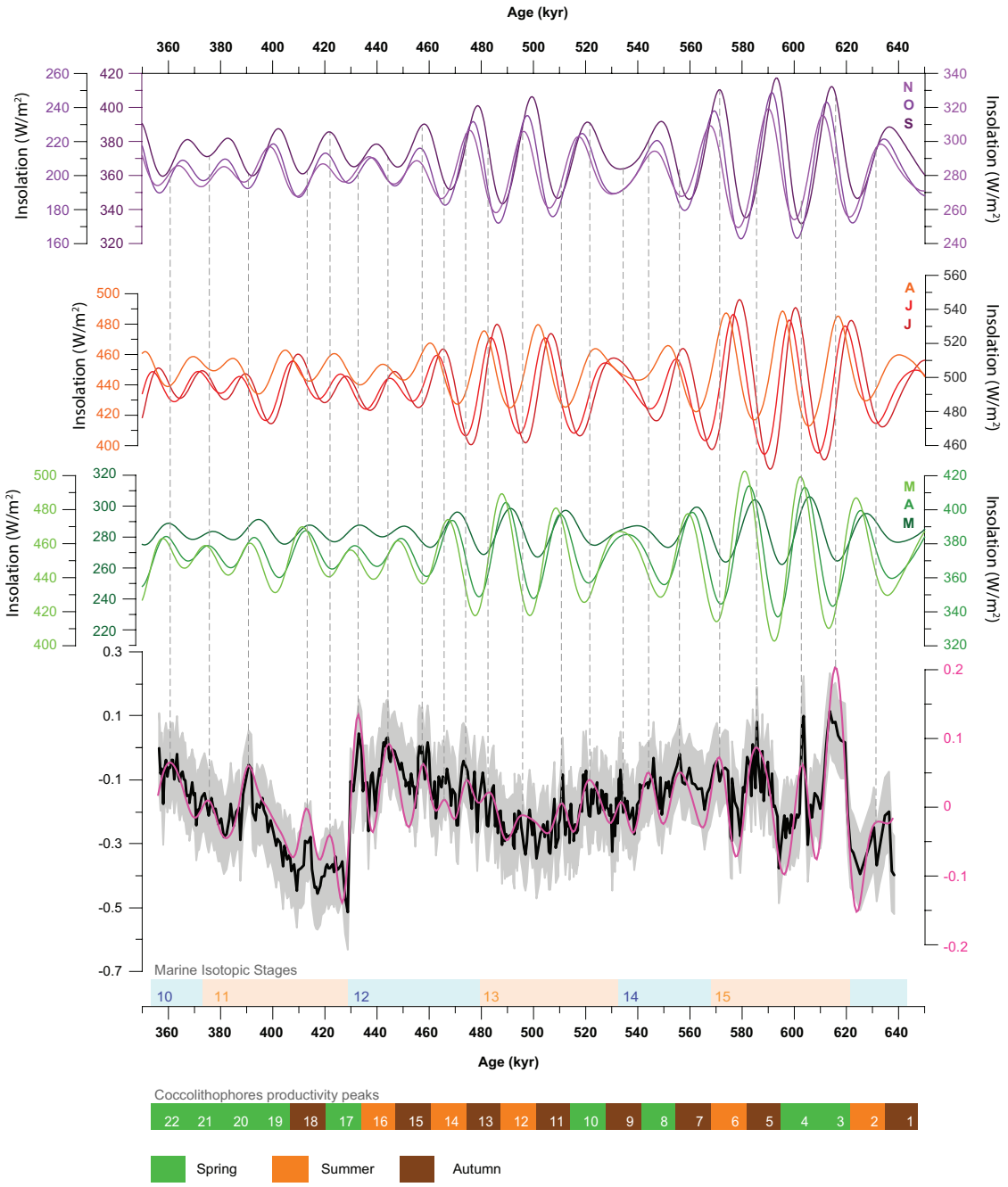

Fig. 10 - Direct comparison between the coccolithophore productivity record (this study) with confidence interval (grey) and a Gaussian bandpass filter (magenta; frequency of 0.07 c/kyr and a bandwidth of 0.05 c/kyr), in comparison to the monthly insolation curves (at 41ºN) from Laskar et al. (2004). Each group of three curves represent a season and each letter the respective month, for example, dark green is March (M), green is April (A) and light green is May (M). Spring is in green tones, Summer in red tones and Autumn in purple tones. Winter insolation curves were not drawn because low insolation and low temperatures would not allow high coccolithophore production.

As mentioned above, the southward migration of the hydrographic fronts drove a southward migration of the high coccolithophorid productivity belt (McIntyre et al., 1972; Villanueva et al., 2001). We therefore hypothesize that the phenology of coccolithophore productivity changed through time and depending on the productive months the resulting coccolithophore productivity record resonated with insolation at different times of the year. In Fig. 10, a color code identifies the season of each production peak to better visualize that during warmer periods, such as MIS 15, MIS 13 and most of MIS 11 the peaks coincided with either spring or autumn, whereas during cold periods, such as in MIS 14 and MIS 12, peaks coincided with summer or autumn.

A comparison of the timing of productivity peaks to insolation reveals that during MIS 15, MIS 13 and MIS 11, productivity peaks coincided either with spring or autumn insolation maxima. This is comparable to the present day, when coccolithophores are most productive in spring and/or autumn (Fig. 1c). On orbital time scales, these productivity peaks are enhanced by insolation, generating an approximate semi-precessional pacing pattern during interglacials. On the other hand, we observe that during MIS 14 and MIS 12, coccolithophore productivity peaks only coincided with summer/autumn insolation maxima (Fig. 10). This fundamental shift in the productivity regime, from interglacial to glacial conditions, breaks the regularity in the precessional forcing and induces non-intuitive unusual periodicities at 15 kyr and 9 kyr (similar to the non-intuitive examples given in Fig. 8c to f). These glacial periodicities provide insight to the origin of the regime shift. It reflects the southward migration of the frontal system, which forces coccolithophores at Site U1313 to change their phenology such that they only bloom once a year during the warm season, similar to what happens today in the subpolar North Atlantic (Fig. 1b). The productivity regime at Site U1313 would thus change from a mid-latitude regime

(similar to Fig. 1c) during interglacials to a subpolar regime (similar to Fig. 1b) during glacials. Such a model with variable phenology would result in two annual productivity peaks approximately 6 months apart, in spring/early-summer and late-summer/autumn during interglacials, whereas during colder periods, and especially during MIS 14 and MIS 12, only one growth season occurred during summer/autumn and the high nutrients/high insolation window for rapid phytoplankton growth was narrower than today.

In all scenarios, productivity peaked whenever insolation was at maximum for the appropriate growth season(s). Productivity peaks during interglacials are thus ~23 kyr and ~11.5 kyr apart, reflecting precession and semi-precession signals associated with the rapid growth seasons of spring and autumn. On the other hand, during glacials peaks are only ~23 kyr apart but shifted in phase by ~6 kyr from the interglacial pattern because the rapid growth season happens later in the year, in summer/autumn (Fig. 10). The studied interval spans a series of successive events (interglacial, glaciation, glacial, termination, etc.) and Fig. 10 demonstrates a phenology shift through time, with higher coccolithophore productivity matching insolation maxima during different seasons. It is this continuous phase shift that results in the observed apparent 15 kyr and 9 kyr periodicities. The continuous adaptation to the best conditions leads to changes in phenology as the timing between peak-growth months changed.

5.4. Comparison with other productivity proxies

Our inference that coccolithophore productivity was generally higher during glacials compared to interglacials is in line with evidence from other primary productivity proxies. Both TOC and total alkenone concentration data from the same site support enhanced primary productivity during glacials, recording higher values during MIS 16, MIS 14 and MIS 12 (Fig. 6a and b). This pattern of increased TOC accumulation during MIS 12 (and MIS 10) and low

678 accumulation during interglacial MIS 11 and MIS 13 was also observed further south at Ocean
679 Drilling Program (ODP) Site 1063 on Bermuda Rise (Poli et al., 2012). At that site, $\delta^{13}C$ of
680 organic matter and benthic foraminifer assemblage data support enhanced glacial marine
681 productivity and constant organic matter flux, partially through delivery of phytodetritus, to the
682 seafloor (Poli et al., 2012). In contrast to the CF Sr/Ca and organic matter evidence, the NAR at
683 Site U1313, spanning MIS 12 to MIS 11 (Fig. 6f; Kulhanek, 2009), reveals higher coccolith
684 accumulation rates during MIS 11 than MIS 12, suggesting that coccolithophore productivity
685 was higher during warmer MIS 11 than during glacial MIS 12. Similar observations based on
686 high coccolith numbers during interglacials were made for the North Atlantic and Norwegian-
687 Greenland Sea (e.g., McIntyre et al., 1972; Henrich and Baumann, 1999; Emanuele et al., 2015).

688 Conditions for both calcium carbonate and organic matter preservation are known to have
689 changed significantly on glacial-interglacial time scales in the North Atlantic basin. The deep
690 North Atlantic was filled by southern sourced waters during glacial periods (Raymo et al., 2004;
691 Curry and Oppo, 2005; Voelker et al., 2010; Poirier and Billups, 2014) as deduced by very low
692 benthic carbon isotopic values in the record from MIS 12 and MIS 16 (Fig. 7a). These southern
693 sourced water masses are poorer in oxygen and richer in CO_2 and thus enhance the preservation
694 of organic matter (Rullkötter, 2006) whilst promoting dissolution of calcium carbonate shells,
695 such as coccoliths. Although there is a consistent decrease in carbonate (and coccolith)
696 accumulation during glacials, our observations indicate that coccolith preservation was good to
697 moderate throughout the studied period. This could explain the seemingly contradictory trends of
698 TOC (and alkenone) concentration and $CaCO_3$ (and NAR) at the studied site (Fig. 6a, b, c, f).
699 Results from the Site 1063 study (Poli et al., 2012) shows that the increased TOC content in the
700 glacial sediments is not purely due to enhanced preservation, but also indicates higher

productivity, supporting our CF Sr/Ca productivity record. Moreover, increased phytoplankton (dinoflagellates) productivity at DSDP Site 607/IODP Site U1313 during the glacial periods around the Plio/Pleistocene transition was also atributed to increased nutrient availability following changes in atmospheric circulation (Versteegh et al., 1996; Hennissen et al., 2017).

The varying extent of southern source water masses would have acted to enhance the preservation of organic matter during times of high productivity, whilst decreasing the preservation of coccolithophore carbonate. We explain the discrepancy between the TOC and NAR proxies at Site U1313 by the relatively small change in carbonate content, which implies that the site remained above the regional lysocline. Indeed, other sites in the North Atlantic, such as ODP Sites 980 and 984 and IODP Site U1314 (Ortiz et al., 1999; Channell and Raymo, 2003; Grützner and Higgins, 2010), at 2180 m, 1660 m and 2820 m water depth, respectively, registered up to 20% reduction in calcium carbonate content during glacial MIS 12. The lower amplitude of change in carbonate signal at Site U1313 (3426 m depth) must therefore also include a component of enhanced carbonate productivity, which was in reality much higher during the glacial at this site and buffered the effect of the more corrosive nature of the bottom water.

6. Conclusions

We use the CF Sr/Ca ratio as a proxy for coccolithophore growth rate and productivity to show that the North Atlantic transitional area was characterized by high-frequency variability in productivity. The dominant glacial-interglacial pattern is explained by changes in circulation and frontal system position that allow enhanced replenishment of nutrients to the surface ocean during glaciations and culminating during glacial maxima. High-frequency suborbital shifts show periodicities of 15 kyr and 9 kyr that are not consistent with orbital forcing. However, a

724 different pattern appears when glacials and interglacials are viewed separately, which reveals a
725 dominant insolation forcing for each, but resonating with different phenology patterns. Thus, we
726 conclude that coccolithophore productivity responded to the interplay between oceanic
727 circulation and insolation. It is important to integrate this into model experiments to assess
728 possible scenarios where coccolithophores may have played a significant role on orbital and
729 suborbital changes in pCO_2.

Acknowledgments

The samples for this study were provided by the Integrated Ocean Drilling Program (IODP, 2003-2013). The study was financially supported by the Fundação para a Ciência e a Tecnologia (FCT; Portugal) through projects INTER-TRACE (PTDC/CLI/70772/2006), PORTO (PDCT/MAR/58282/2004) and CCMAR (UID/Multi/04326/2013). Funding for XRF core scanning by J.G. was provided by the Deutsche Forschungsgemeinschaft through grant We 992/49. C.C. acknowledges her doctoral fellowship (SFRH/BD/84187/2012) and A.V. her FCT Investigador contract (IF/01500/2014). C.C. also acknowledges the laboratorial and analytical support at the Geosciences Department, University of Oviedo, and at MARUM and Geosciences Department, University of Bremen. C.C. would like to thank Dr. Manfred Mudelsee on the methodology applied for the time frequency analysis and Dr. David de Vleeschouwer for his help with the Monte Carlo simulation. We also acknowledge the positive comments and suggestions of the two reviewers that resulted in an improved manuscript. The data used is available from the Pangaea data repository under parent link https://doi.pangaea.de/10.1594/PANGAEA.

References

Alonso-Garcia, M., Sierro, F.J., Flores, J.A., 2011. Arctic front shifts in the subpolar North Atlantic during the Mid-Pleistocene (800–400ka) and their implications for ocean circulation. Palaeogeogr. Palaeoclimatol. Palaeoecol. 311, 268–280. https://doi.org/10.1016/j.palaeo.2011.09.004

Andruleit, H., 1996. A Filtration Technique for Quantitative Studies of Coccoliths. Micropaleontology 42, 403. https://doi.org/10.2307/1485964

Antoine, D., André, J.-M., Morel, A., 1996. Oceanic primary production: 2. Estimation at global scale from satellite (Coastal Zone Color Scanner) chlorophyll. Global Biogeochem.

754 Cycles 10, 57–69. https://doi.org/10.1029/95GB02832
755 Antoine, D., Morel, A., 1996a. Oceanic primary production: 1. Adaptation of a spectral
756 light-photosynthesis model in view of application to satellite chlorophyll observations. Global
757 Biogeochem. Cycles 10, 43–55. https://doi.org/10.1029/95GB02831
758 Balch, W.M., 2004. Re-evaluation of the physiological ecology of coccolithophores BT -
759 Coccolithophores: From Molecular Processes to Global Impact, in: Thierstein, H.R., Young, J.R.
760 (Eds.), . Springer Berlin Heidelberg, Berlin, Heidelberg, pp. 165–190.
761 https://doi.org/10.1007/978-3-662-06278-4_7
762 Barbosa, A.B., 2009. Dynamics of living phytoplankton: Implications for
763 paleoenvironmental reconstructions. IOP Conf. Ser. Earth Environ. Sci. 5, 12001.
764 https://doi.org/10.1088/1755-1307/5/1/012001
765 Barker, S., Archer, D., Booth, L., Elderfield, H., Henderiks, J., Rickaby, R.E.M., 2006.
766 Globally increased pelagic carbonate production during the Mid-Brunhes dissolution interval and
767 the CO_2 paradox of MIS 11. Quat. Sci. Rev. 25, 3278–3293.
768 https://doi.org/http://dx.doi.org/10.1016/j.quascirev.2006.07.018
769 Barton, A., Greene, C., Monger, B., Pershing, A., 2003. The Continuous Plankton
770 Recorder survey and the North Atlantic Oscillation: Interannual- to Multidecadal-scale patterns
771 of phytoplankton variability in the North Atlantic Ocean. Prog. Oceanogr. 58, 337–358.
772 https://doi.org/10.1016/j.pocean.2003.08.012
773 Baumann, K.-H., Andruleit, H., Böckel, B., Geisen, M., Kinkel, H., 2005. The significance
774 of extant coccolithophores as indicators of ocean water masses, surface water temperature, and
775 palaeoproductivity: a review. Paläontologische Zeitschrift 79, 93–112.
776 https://doi.org/10.1007/BF03021756
777 Baumann, K.-H., Andruleit, H., Samtleben, C., 2000. Coccolithophores in the Nordic Seas:
778 comparison of living communities with surface sediment assemblages. Deep Sea Res. Part II
779 Top. Stud. Oceanogr. 47, 1743–1772. https://doi.org/10.1016/s0967-0645(00)00005-9
780 Baumann, K.-H., Freitag, T., 2004. Pleistocene fluctuations in the northern Benguela
781 Current system as revealed by coccolith assemblages. Mar. Micropaleontol. 52, 195–215.
782 https://doi.org/10.1016/j.marmicro.2004.04.011
783 Berger, A., 1988. Milankovitch Theory and climate. Rev. Geophys. 26, 624–657.
784 https://doi.org/doi:10.1029/RG026i004p00624

785 Bollmann, J., Baumann, K.-H., Thierstein, H.R., 1998. Global dominance of Gephyrocapsa
786 coccoliths in the Late Pleistocene: Selective dissolution, evolution, or global environmental
787 change? Paleoceanography 13, 517–529. https://doi.org/10.1029/98PA00610
788 Bolton, C., Hernández-Sánchez, M.T., Fuertes, M.-Á., González-Lemos, S., Abrevaya, L.,
789 Mendez-Vicente, A., Flores, J.-A., Probert, I., Giosan, L., Johnson, J., Stoll, H.M., 2016.
790 Decrease in coccolithophore calcification and CO_2 since the middle Miocene. Nat. Commun. 7,
791 10284.
792 Brand, L.E., 1994. Physiological ecology of marine coccolithophores, in: Winter, A.,
793 Siesser, W.G. (Eds.), Coccolithophores. Cambridge University Press, pp. 39–49.
794 Broerse, A. T. C., Ziveri, P., van Hinte, J. E., Honjo, S., 2000. Coccolithophore export
795 production, species composition, and coccolith $CaCO_3$ fluxes in the NE Atlantic (34°N 21°W
796 and 48°N 21°W). Deep-Sea Res. II, 47, 1877-1905.
797 Cabarcos, E., Flores, J.-A., Sierro, F.J., 2014. High-resolution productivity record and
798 reconstruction of ENSO dynamics during the Holocene in the Eastern Equatorial Pacific using
799 coccolithophores. The Holocene 24, 176–187. https://doi.org/10.1177/0959683613516818
800 Cavaleiro, C.D., 2011. Paleo-productivity changes in the North Atlantic (IODP Site
801 U1313) during Marine Isotopic Stages (MIS) 10 to 12 based on nannofossil Sr/Ca data.
802 University of Oviedo.
803 Channell, J.E.T., Kanamatsu, T., Sato, T., Stein, R., Alvarez Zarikian, C.A., Malone, M.J.,
804 Scientists, E. 303/306, 2006. Expedition Reports North Atlantic Climate. Exped. Reports North
805 Atl. Clim. Integr. Ocean Drill. Progr. Manag. Int. Inc., Coll. Stn. TX Volume 303.
806 Channell, J.E.T., Raymo, M.E., 2003. Paleomagnetic record at ODP Site 980 (Feni Drift,
807 Rockall) for the past 1.2 Myrs. Geochemistry, Geophys. Geosystems 4, 1–14.
808 https://doi.org/10.1029/2002GC000440
809 Curry, W.B., Oppo, D.W., 2005. Glacial water mass geometry and the distribution of $\delta^{13}C$
810 of ΣCO_2 in the western Atlantic Ocean. Paleoceanography 20, PA1017.
811 https://doi.org/10.1029/2004PA001021
812 de Villiers, S., Greaves, M., Elderfield, H., 2002. An intensity ratio calibration method for
813 the accurate determination of Mg/Ca and Sr/Ca of marine carbonates by ICP-AES. Geochem.,
814 Geophys. Geosystems 3, 2001GC000169
815 Dittert, N., Baumann, K.-H., Bickert, T., Henrich, R., Huber, R., Kinkel, H., Meggers, H.,

1999. Carbonate Dissolution in the Deep-Sea: Methods, Quantification and Paleoceanographic Application BT - Use of Proxies in Paleoceanography: Examples from the South Atlantic, in: Fischer, G., Wefer, G. (Eds.). Springer Berlin Heidelberg, Berlin, Heidelberg, pp. 255–284. https://doi.org/10.1007/978-3-642-58646-0_10

Emanuele, D., Ferretti, P., Palumbo, E., Amore, F.O., 2015. Sea-surface dynamics and palaeoenvironmental changes in the North Atlantic Ocean (IODP Site U1313) during Marine Isotope Stage 19 inferred from coccolithophore assemblages. Palaeogeogr. Palaeoclimatol. Palaeoecol. 430, 104–117. https://doi.org/10.1016/j.palaeo.2015.04.014

Falkowski, P.G., Ziemann, D., Kolber, Z., Bienfang, P.K., 1991. Role of eddy pumping in enhancing primary production in the ocean. Nature 352, 55–58. https://doi.org/10.1038/352055a0

Fasham, M.J.R., Platt, T., Irwin, B., Jones, K., 1985. Factors affecting the spatial pattern of the deep chlorophyll maximum in the region of the Azores front. Prog. Oceanogr. 14, 129–165. https://doi.org/10.1016/0079-6611(85)90009-6

Fink, C., Baumann, K.-H., Groeneveld, J., Steinke, S., 2010. Strontium/Calcium ratio, carbon and oxygen stable isotopes in coccolith carbonate from different grain-size fractions in South Atlantic surface sediments. Geobios 43, 151–164. https://doi.org/10.1016/j.geobios.2009.11.001

Flores, J.-A., Marino, M., Sierro, F.J., Hodell, D.A., Charles, C.D., 2003. Calcareous plankton dissolution pattern and coccolithophore assemblages during the last 600 kyr at ODP Site 1089 (Cape Basin, South Atlantic): paleoceanographic implications. Palaeogeogr. Palaeoclimatol. Palaeoecol. 196, 409–426. https://doi.org/10.1016/S0031-0182(03)00467-X

Frank, N., Freiwald, A., Correa, M.L., Wienberg, C., Eisele, M., Hebbeln, D., Van Rooij, D., Henriet, J.-P., Colin, C., van Weering, T., de Haas, H., Buhl-Mortensen, P., Roberts, J.M., De Mol, B., Douville, E., Blamart, D., Hatte, C., 2011. Northeastern Atlantic cold-water coral reefs and climate. Geology 39, 743–746. https://doi.org/10.1130/G31825.1

Fratantoni, D.M., 2001. North Atlantic surface circulation during the 1990's observed with satellite-tracked drifters. J. Geophys. Res. 106, 22067. https://doi.org/10.1029/2000JC000730

Grützner, J., Higgins, S.M., 2010. Threshold behavior of millennial scale variability in deep water hydrography inferred from a 1.1 Ma long record of sediment provenance at the southern Gardar Drift. Paleoceanography 25, 2009PA001873

Hays, J.D., Imbrie, J., Shackleton, N.J., 1976. Variations in the Earth's Orbit: Pacemaker of the Ice Ages. Science 194, 1121–1132. 10.1126/science.194.4270.1121

Hennissen, J.A.I., Head, M.J., De Schepper, S., Groeneveld, J., 2017. Dinoflagellate cyst paleoecology during the Pliocene–Pleistocene climatic transition in the North Atlantic. Palaeogeogr. Palaeoclimatol. Palaeoecol. 470, 81–108. https://doi.org/https://doi.org/10.1016/j.palaeo.2016.12.023

Henrich, R. and Baumann, K.-H., 1994. Evolution of the Norwegian Current and the Scandinavian Ice Sheets during the past 2.6 Mys: evidence from ODP Leg 104 biogenic carbonate and terrigenous records. Palaeogeogra., Palaeoclimatol., Palaeoecol.108, 75–94.

Henson, S.A., Dunne, J.P., Sarmiento, J.L., 2009. Decadal variability in North Atlantic phytoplankton blooms. J. Geophys. Res. 114, C04013. https://doi.org/10.1029/2008JC005139

Herbert, T.D., Sarmiento, J.L., 1991. Ocean nutrient distribution and oxygenation: Limits on the formation of warm saline bottom water over the past 91 m.y. Geology 19, 702–705.

Jansen, J.H.F., Kuijpers, A., Troelstra, S.R., 1986. A Mid-Brunhes Climatic Event: Long-Term Changes in Global Atmosphere and Ocean Circulation. Science 232, 619–622. https://doi.org/10.1126/science.232.4750.619

Johannessen, T., Jansen, E., Flatøy, A., Ravelo, A.C., 1994. The Relationship between Surface Water Masses, Oceanographic Fronts and Paleoclimatic Proxies in Surface Sediments of the Greenland, Iceland, Norwegian Seas, in: Zahn, R., Pedersen, T.F., Kaminski, M.A., Labeyrie, L. (Eds.), Carbon Cycling in the Glacial Ocean: Constraints on the Ocean's Role in Global Change: Quantitative Approaches in Paleoceanography. Springer Berlin Heidelberg, Berlin, Heidelberg, pp. 61–85. https://doi.org/10.1007/978-3-642-78737-9_4

Jouzel, J., Masson-Delmotte, V., Cattani, O., Dreyfus, G., Falourd, S., Hoffmann, G., Minster, B., Nouet, J., Barnola, J.M., Chappellaz, J., Fischer, H., Gallet, J.C., Johnsen, S., Leuenberger, M., Loulergue, L., Luethi, D., Oerter, H., Parrenin, F., Raisbeck, G., Raynaud, D., Schilt, A., Schwander, J., Selmo, E., Souchez, R., Spahni, R., Stauffer, B., Steffensen, J.P., Stenni, B., Stocker, T.F., Tison, J.L., Werner, M., Wolff, E.W., 2007. Orbital and Millennial Antarctic Climate Variability over the Past 800,000 Years. Science 317, 793–796. https://doi.org/10.1126/science.1141038

Kucera, M., Rosell-Melé, A., Schneider, R., Waelbroeck, C., Weinelt, M., 2005. Multiproxy approach for the reconstruction of the glacial ocean surface (MARGO). Quat. Sci.

878 Rev. 24, 813–819. https://doi.org/http://dx.doi.org/10.1016/j.quascirev.2004.07.017
879 Kulhanek, D.K., 2009. Calcareous nannoplankton as paleoceanographic and
880 biostratigraphic proxies: examples from the Mid-Cretaceous Equatorial Atlantic (ODP Leg 207),
881 Pleistocene of the Antarctic Peninsula (NBP0602A) and North Atlantic (IODP Exp.306). Florida
882 State University.
883 Laskar, J., Robutel, P., Joutel, F., Gastineau, M., Correia, A.C.M., Levrard, B., 2004. A
884 long-term numerical solution for the insolation quantities of the Earth. Astron. Astrophys. 428,
885 261–285. https://doi.org/10.1051/0004-6361:20041335
886 Lévy, M., 2005. Production regimes in the northeast Atlantic: A study based on Sea-
887 viewing Wide Field-of-view Sensor (SeaWiFS) chlorophyll and ocean general circulation model
888 mixed layer depth. J. Geophys. Res. 110, C07S10. https://doi.org/10.1029/2004JC002771
889 Lisiecki, L.E., Raymo, M.E., 2005. A Pliocene-Pleistocene stack of 57 globally distributed
890 benthic δ 18 O records. Paleoceanography 20. https://doi.org/10.1029/2004PA001071
891 Longhurst, A., 1995. Seasonal cycles of pelagic production and consumption. Prog.
892 Oceanogr. 36, 77–167. https://doi.org/10.1016/0079-6611(95)00015-1
893 Longhurst, A., Sathyendranath, S., Platt, T., Caverhill, C., 1995a. An estimate of global
894 primary production in the ocean from satellite radiometer data. J. Plankton Res. 17, 1245–1271.
895 https://doi.org/10.1093/plankt/17.6.1245
896 Longhurst, A.R., 2007. THE ATLANTIC OCEAN, in: Longhurst, A.R. (Ed.), Ecological
897 Geography of the Sea. Elsevier, Burlington, pp. 131–273. https://doi.org/10.1016/B978-
898 012455521-1/50010-3
899 Loutre, M.F., Berger, A., 2003. Marine Isotope Stage 11 as an analogue for the present
900 interglacial. Glob. Planet. Change 36, 209–217. https://doi.org/http://dx.doi.org/10.1016/S0921-
901 8181(02)00186-8
902 Maiorano, P., Marino, M., Balestra, B., Flores, J.-A., Hodell, D.A., Rodrigues, T., 2015.
903 Coccolithophore variability from the Shackleton Site (IODP Site U1385) through MIS 16-10.
904 Glob. Planet. Change 133, 35–48. https://doi.org/https://doi.org/10.1016/j.gloplacha.2015.07.009
905 Malone, M.J., Baker, P.A., 1999. Temperature dependence of the strontium distribution
906 coefficient in calcite: an experimental study from 40° to 200 °C and application to natural
907 diagenetic calcites. J. Sediment. Res. 69.
908 Marino, M., Maiorano, P., Lirer, F., 2008. Changes in calcareous nannofossil assemblages

909 during the Mid-Pleistocene Revolution. Mar. Micropaleontol. 69, 70–90.
910 https://doi.org/https://doi.org/10.1016/j.marmicro.2007.11.010
911 Marino, M., Maiorano, P., Tarantino, F., Voelker, A., Capotondi, L., Girone, A., Lirer, F.,
912 Flores, J.-A., Naafs, B.D.A., 2014. Coccolithophores as proxy of seawater changes at orbital-to-
913 millennial scale during middle Pleistocene Marine Isotope Stages 14-9 in North Atlantic core
914 MD01-2446. Paleoceanography 29, 518–532. https://doi.org/10.1002/2013PA002574
915 Marinov, I., Doney, S.C., Lima, I.D., 2010. Response of ocean phytoplankton community
916 structure to climate change over the 21st century: partitioning the effects of nutrients,
917 temperature and light. Biogeosciences 7, 3941–3959. https://doi.org/10.5194/bg-7-3941-2010
918 Martin, J.H., Gordon, R.M., Fitzwater, S.E., 1990. Iron in Antarctic waters. Nature 345,
919 156–158. https://doi.org/10.1038/345156a0
920 Maslin, M.A., Shackleton, N.J., Pflaumann, U., 1995. Surface water temperature, salinity,
921 and density changes in the northeast Atlantic during the last 45,000 years: Heinrich events, deep
922 water formation, and climatic rebounds. Paleoceanography 10, 527–544.
923 https://doi.org/10.1029/94PA03040
924 McIntyre, A., Ruddiman, W.F., Jantzen, R., 1972. Southward penetrations of the North
925 Atlantic polar front: faunal and floral evidence of large-scale surface water mass movements
926 over the last 225,000 years. Deep Sea Res. Oceanogr. Abstr. 19, 61–77.
927 https://doi.org/10.1016/0011-7471(72)90073-3
928 Mejía, L.M., Ziveri, P., Cagnetti, M., Bolton, C., Zahn, R., Marino, G., Martínez-Méndez,
929 G., Stoll, H., 2014. Effects of midlatitude westerlies on the paleoproductivity at the Agulhas
930 Bank slope during the penultimate glacial cycle: Evidence from coccolith Sr/Ca ratios.
931 Paleoceanography 29, 697–714. https://doi.org/10.1002/2013PA002589
932 Meyers, S.R., 2014. Astrochron: An R Package for Astrochronology. https://cran.r-
933 project.org/package=astrochron
934 Mudelsee, M., 2014. Climate Time Series Analysis - Classical Statistical and Bootstrap
935 Methods, 2nd ed, Atmospheric and Oceanographic Sciences Library. Springer International
936 Publishing. https://doi.org/10.1007/978-3-319-04450-7
937 Müller, M.N., Lebrato, M., Riebesell, U., Barcelos e Ramos, J., Schulz, K.G., Blanco-
938 Ameijeiras, S., Sett, S., Eisenhauer, A., Stoll, H.M., 2014. Influence of temperature and CO_2 on
939 the strontium and magnesium composition of coccolithophore calcite. Biogeosciences 11, 1065–

1075. https://doi.org/10.5194/bg-11-1065-2014

Müller, M.N., Trull, T.W., Hallegraeff, G.M., 2017. Independence of nutrient limitation and carbon dioxide impacts on the Southern Ocean coccolithophore Emiliania huxleyi. Isme J. 11, 1777.

Naafs, B.D.A., Hefter, J., Acton, G., Haug, G.H., Martínez-Garcia, A., Pancost, R., Stein, R., 2012. Strengthening of North American dust sources during the late Pliocene (2.7Ma). Earth Planet. Sci. Lett. 317–318, 8–19. https://doi.org/10.1016/j.epsl.2011.11.026

Naafs, B.D.A., Hefter, J., Ferretti, P., Stein, R., Haug, G.H., 2011. Sea surface temperatures did not control the first occurrence of Hudson Strait Heinrich Events during MIS 16. Paleoceanography 26.

Nimer, N.A., Merrett, M.J., 1993. Calcification rate in Emiliania huxleyi Lohmann in response to light, nitrate and availability of inorganic carbon. New Phytol. 123, 673–677. https://doi.org/10.1111/j.1469-8137.1993.tb03776.x

Omta, A.W., K. van Voorn, G.A., M. Rickaby, R.E., Follows, M.J., 2013. On the potential role of marine calcifiers in glacial-interglacial dynamics. Global Biogeochem. Cycles 27, 692–704. https://doi.org/10.1002/gbc.20060

Oppo, D.W., McManus, J.F., Cullen, J.L., 1998. Abrupt Climate Events 500,000 to 340,000 Years Ago: Evidence from Subpolar North Atlantic Sediments. Science 279, 1335–1338. https://doi.org/10.1126/science.279.5355.1335

Ortiz, J., Mix, A., Harris, S., O'Connell, S., 1999. Diffuse spectral reflectance as a proxy for percent carbonate content in North Atlantic sediments. Paleoceanography 14, 171–186. https://doi.org/10.1029/1998PA900021

Oschlies, A., 2002. Can eddies make ocean deserts bloom? Global Biogeochem. Cycles 16, 53-1-53–11. https://doi.org/10.1029/2001GB001830

Oschlies, A., Garçon, V., 1998. Eddy-induced enhancement of primary production in a model of the North Atlantic Ocean. Nature 394, 266–269. https://doi.org/10.1038/28373

Paillard, D., Labeyrie, L., Yiou, P., 1996. Macintosh Program performs time-series analysis. Eos, Trans. Am. Geophys. Union 77, 379–379. https://doi.org/10.1029/96EO00259

Pisias, N.G., Dauphin, J.P., Sancetta, C., 1973. Spectral analysis of late Pleistocene-Holocene sediments. Quat. Res. 3, 3–9. https://doi.org/10.1016/0033-5894(73)90050-1

Poirier, R.K., Billups, K., 2014. The intensification of northern component deepwater

971 formation during the mid-Pleistocene climate transition. Paleoceanography 29, 1046–1061.
972 https://doi.org/10.1002/2014PA002661
973 Poli, M.S., Meyers, P.A., Thunell, R.C., Capodivacca, M., 2012. Glacial-interglacial
974 variations in sediment organic carbon accumulation and benthic foraminiferal assemblages on
975 the Bermuda Rise (ODP Site 1063) during MIS 13 to 10. Paleoceanography 27.
976 https://doi.org/10.1029/2012PA002314
977 Priede, I.G., Billett, D.S.M., Brierley, A.S., Hoelzel, A.R., Inall, M., Miller, P.I., Cousins,
978 N.J., Shields, M.A., Fujii, T., 2013. The ecosystem of the Mid-Atlantic Ridge at the sub-polar
979 front and Charlie–Gibbs Fracture Zone; ECO-MAR project strategy and description of the
980 sampling programme 2007–2010. Deep Sea Res. Part II Top. Stud. Oceanogr. 98, 220–230.
981 https://doi.org/10.1016/j.dsr2.2013.06.012
982 Raffi, I., Backman, J., Fornaciari, E., Pälike, H., Rio, D., Lourens, L., Hilgen, F., 2006. A
983 review of calcareous nannofossil astrobiochronology encompassing the past 25 million years.
984 Quat. Sci. Rev. 25, 3113–3137. https://doi.org/https://doi.org/10.1016/j.quascirev.2006.07.007
985 Rahmstorf, S., 2002. Ocean circulation and climate during the past 120,000 years. Nature
986 419, 207–214. https://doi.org/10.1038/nature01090
987 Raymo, M.E., Oppo, D.W., Flower, B.P., Hodell, D.A., McManus, J.F., Venz, K.A.,
988 Kleiven, K.F., McIntyre, K., 2004. Stability of North Atlantic water masses in face of
989 pronounced climate variability during the Pleistocene. Paleoceanography 19, PA2008.
990 https://doi.org/10.1029/2003PA000921
991 Reverdin, G., 2003. North Atlantic Ocean surface currents. J. Geophys. Res. 108, 3002.
992 https://doi.org/10.1029/2001JC001020
993 Rickaby, R.E.M., Bard, E., Sonzogni, C., Rostek, F., Beaufort, L., Barker, S., Rees, G.,
994 Schrag, D.P., 2007. Coccolith chemistry reveals secular variations in the global ocean carbon
995 cycle? Earth Planet. Sci. Lett. 253, 83–95. https://doi.org/10.1016/j.epsl.2006.10.016
996 Rickaby, R.E.M., Elderfield, H., Roberts, N., Hillenbrand, C.-D., Mackensen, A., 2010.
997 Evidence for elevated alkalinity in the glacial Southern Ocean. Paleoceanography 25.
998 https://doi.org/10.1029/2009PA001762
999 Rodrigues, T., Alonso-García, M., Hodell, D.A., Rufino, M., Naughton, F., Grimalt, J.O.,
1000 Voelker, A.H.L., Abrantes, F., 2017. A 1-Ma record of sea surface temperature and extreme
1001 cooling events in the North Atlantic: A perspective from the Iberian Margin. Quat. Sci. Rev. 172,

1002 118–130. https://doi.org/https://doi.org/10.1016/j.quascirev.2017.07.004
1003 Rossby, T., 1999. On gyre interactions. Deep Sea Res. Part II Top. Stud. Oceanogr. 46,
1004 139–164. https://doi.org/10.1016/S0967-0645(98)00095-2
1005 Rost, B., Riebesell, U., 2004. Coccolithophores and the biological pump: responses to
1006 environmental changes, in: Coccolithophores. Springer Berlin Heidelberg, Berlin, Heidelberg,
1007 pp. 99–125. https://doi.org/10.1007/978-3-662-06278-4_5
1008 Ruddiman, W.F., Raymo, M.E., Martinson, D.G., Clement, B.M., Backman, J., 1989.
1009 Pleistocene evolution: Northern hemisphere ice sheets and North Atlantic Ocean.
1010 Paleoceanography 4, 353–412. https://doi.org/10.1029/PA004i004p00353
1011 Rühlemann, C., Müller, P.J., Schneider, R.R., 1999. Organic Carbon and Carbonate as
1012 Paleoproductivity Proxies: Examples from High and Low Productivity Areas of the Tropical
1013 Atlantic BT - Use of Proxies in Paleoceanography: Examples from the South Atlantic, in:
1014 Fischer, G., Wefer, G. (Eds.). Springer Berlin Heidelberg, Berlin, Heidelberg, pp. 315–344.
1015 https://doi.org/10.1007/978-3-642-58646-0_12
1016 Rullkötter, J., 2006. Organic Matter: The Driving Force for Early Diagenesis, in: Marine
1017 Geochemistry. Springer-Verlag, Berlin/Heidelberg, pp. 125–168. https://doi.org/10.1007/3-540-
1018 32144-6_4
1019 Saavedra-Pellitero, M., Baumann, K.-H., Ullermann, J., Lamy, F., 2017. Marine Isotope
1020 Stage 11 in the Pacific sector of the Southern Ocean; a coccolithophore perspective. Quat. Sci.
1021 Rev. 158, 1–14. https://doi.org/https://doi.org/10.1016/j.quascirev.2016.12.020
1022 Schlitzer, R. 2015. Ocean Data View, http://odv.awi.de, 2015.
1023 Schoepfer, S.D., Shen, J., Wei, H., Tyson, R. V, Ingall, E., Algeo, T.J., 2015. Total organic
1024 carbon, organic phosphorus, and biogenic barium fluxes as proxies for paleomarine productivity.
1025 Earth-Science Rev. 149, 23–52. https://doi.org/https://doi.org/10.1016/j.earscirev.2014.08.017
1026 Schulz, M., Mudelsee, M., 2002. REDFIT: estimating red-noise spectra directly from
1027 unevenly spaced paleoclimatic time series. Comput. Geosci. 28, 421–426.
1028 https://doi.org/10.1016/S0098-3004(01)00044-9
1029 Schulz, M., Stattegger, K., 1997. Spectrum: spectral analysis of unevenly spaced
1030 paleoclimatic time series. Comput. Geosci. 23, 929–945. https://doi.org/10.1016/S0098-
1031 3004(97)00087-3
1032 Schwab, C., Kinkel, H., Weinelt, M., Repschläger, J., 2012. Coccolithophore

paleoproductivity and ecology response to deglacial and Holocene changes in the Azores Current System. Paleoceanography 27. https://doi.org/10.1029/2012PA002281

Sigman, D.M., Boyle, E.A., 2000. Glacial/interglacial variations in atmospheric carbon dioxide. Nature 407, 859–869. https://doi.org/10.1038/35038000

Sigman, D.M., McCorkle, D.C., Martin, W.R., 1998. The calcite lysocline as a constraint on glacial/interglacial low-latitude production changes. Global Biogeochem. Cycles 12, 409–427. https://doi.org/10.1029/98GB01184

Stein, R., Hefter, J., Grützner, J., Voelker, A., Naafs, B.D.A., 2009. Variability of surface water characteristics and Heinrich-like events in the Pleistocene midlatitude North Atlantic Ocean: Biomarker and XRD records from IODP Site U1313 (MIS 16-9). Paleoceanography 24. https://doi.org/10.1029/2008PA001639

Stein, R., Kanamatsu, T., Alvarez-Zarikian, C., Higgins, S.M., Channell, J.E.T., Aboud, E., Ohno, M., Acton, G.D., Akimoto, K., Bailey, I., Bjørklund, K.R., Evans, H., Nielsen, S.H.H., Fang, N., Ferretti, P., Gruetzner, J., Guyodo, Y.J.B., Hagino, K., Harris, R., Hatakeda, K., Hefter, J., Judge, S.A., Kulbanek, D.K., Nanayama, F., Rashid, H., Sanchez, F.J.S., Voelker, A., Zhai, Q., 2006. North Atlantic paleoceanography: The last five million years. Eos, Trans. Am. Geophys. Union 87, 129–133. https://doi.org/10.1029/2006EO130002

Stoll, H., Shimizu, N., Arevalos, A., Matell, N., Banasiak, A., Zeren, S., 2007. Insights on coccolith chemistry from a new ion probe method for analysis of individually picked coccoliths. Geochemistry, Geophys. Geosystems 8, (6). https://doi.org/10.1029/2006GC001546

Stoll, H.M., Klaas, C.M., Probert, I., Encinar, J.R., Alonso, J.I.G., 2002a. Calcification rate and temperature effects on Sr partitioning in coccoliths of multiple species of coccolithophorids in culture. Glob. Planet. Change 34, 153–171. https://doi.org/10.1016/S0921-8181(02)00112-1

Stoll, H.M., Schrag, D.P., 2000. Coccolith Sr/Ca as a new indicator of coccolithophorid calcification and growth rate. Geochemistry, Geophys. Geosystems 1, (5). https://doi.org/10.1029/1999GC000015

Stoll, H.M., Ziveri, P., 2002. Separation of monospecific and restricted coccolith assemblages from sediments using differential settling velocity. Mar. Micropaleontol. 46, 209–221. https://doi.org/10.1016/S0377-8398(02)00040-3

Stoll, H.M., Ziveri, P., M., G., Probert, I., Young, J.R., 2002b. Potential and limitations of Sr/Ca ratios in coccolith carbonate: new perspectives from cultures and monospecific samples

1064 from sediments. Philos. Trans. R. Soc. A Math. Phys. Eng. Sci. 360, 719–747.
1065 https://doi.org/10.1098/rsta.2001.0966
1066 Su, X.,1996. Development of late Tertiary and Quaternary coccolith assemblages in the
1067 northeast Atlantic, GEOMAR Rept, 48, 120pp.
1068 Tangunan, D., Baumann, K.-H., Pätzold, J., Henrich, R., Kucera, M., De Pol-Holz, R.,
1069 Groeneveld, J., 2017. Insolation forcing of coccolithophore productivity in the western tropical
1070 Indian Ocean over the last two glacial-interglacial cycles. Paleoceanography 32, 692–709.
1071 https://doi.org/10.1002/2017PA003102
1072 Thunell, R.C., Poli, M.S., Rio, D., 2002. Changes in deep and intermediate water
1073 properties in the western North Atlantic during marine isotope stages 11–12: evidence from
1074 (ODP) Leg 172. Mar. Geol. 189, 63–77. https://doi.org/http://dx.doi.org/10.1016/S0025-
1075 3227(02)00323-7
1076 Toggweiler, J.R., 2009. Ocean Circulation: Meridional Overturning Circulation A2 -
1077 Steele, John H. BT - Encyclopedia of Ocean Sciences (Second Edition). Academic Press,
1078 Oxford, pp. 126–131. https://doi.org/https://doi.org/10.1016/B978-012374473-9.00596-8
1079 Tyrrell, T., Young, J.R., 2009. Coccolithophores, in: Encyclopedia of Ocean Sciences.
1080 Elsevier, pp. 606–614. https://doi.org/10.1016/B978-012374473-9.00662-7
1081 Vallina, S.M., Simó, R., 2007. Strong Relationship Between DMS and the Solar Radiation
1082 Dose over the Global Surface Ocean. Science 315, 506–508.
1083 Versteegh, G.J.M., Brinkhuis, H., Visscher, H., Zonneveld, K.A.F., 1996. The relation
1084 between productivity and temperature in the Pliocene North Atlantic at the onset of northern
1085 hemisphere glaciation: a palynological study. Glob. Planet. Change 11, 155–165.
1086 https://doi.org/https://doi.org/10.1016/0921-8181(95)00054-2
1087 Villanueva, J., Calvo, E., Pelejero, C., Grimalt, J.O., Boelaert, A., Labeyrie, L., 2001. A
1088 latitudinal productivity band in the central North Atlantic over the last 270 kyr: An alkenone
1089 perspective. Paleoceanography 16, 617–626. https://doi.org/10.1029/2000PA000543
1090 Voelker, A.H.L., de Abreu, L., Schönfeld, J., Erlenkeuser, H., Abrantes, F., 2009.
1091 Hydrographic conditions along the western Iberian margin during marine isotope stage 2.
1092 Geochemistry, Geophys. Geosystems 10. https://doi.org/10.1029/2009GC002605
1093 Voelker, A.H.L., Rodrigues, T., Billups, K., Oppo, D., McManus, J., Stein, R., Hefter, J.,
1094 Grimalt, J.O., 2010. Variations in mid-latitude North Atlantic surface water properties during the

mid-Brunhes (MIS 9–14) and their implications for the thermohaline circulation. Clim. Past 6, 531–552. https://doi.org/10.5194/cp-6-531-2010

Weeks, A., Conte, M.H., Harris, R.P., Bedo, A., Bellan, I., Burkill, P.H., Edwards, E.S., Harbour, D.S., Kennedy, H., Llewellyn, C., Mantoura, R.F.C., Morales, C.E., Pomroy, A.J., Turley, C.M., 1993. The physical and chemical environment and changes in community structure associated with bloom evolution: the Joint Global Flux Study North Atlantic Bloom Experiment. Deep Sea Res. Part II Top. Stud. Oceanogr. 40, 347–368. https://doi.org/10.1016/0967-0645(93)90021-E

Wefer, G., Berger, W.H., Bijma, J., Fischer, G., 1999. Clues to Ocean History: a Brief Overview of Proxies BT - Use of Proxies in Paleoceanography: Examples from the South Atlantic, in: Fischer, G., Wefer, G. (Eds.). Springer Berlin Heidelberg, Berlin, Heidelberg, pp. 1–68. https://doi.org/10.1007/978-3-642-58646-0_1

Wright, A.K., Flower, B.P., 2002. Surface and deep ocean circulation in the subpolar North Atlantic during the Mid-Pleistocene revolution. Paleoceanography 17 (4), 1068. http://dx.doi.org/10.1029/2002PA000782.

Young, J., Geisen, M., Cros, L., Kleijne, A., Sprengel, C., Probert, I., Ostergaard, J., 2003. A guide to extant coccolithophore taxonomy. J. Nannoplankt. Res. Special Is, 125 p.

Young, J.R., Ziveri, P., 2000. Calculation of coccolith volume and it use in calibration of carbonate flux estimates. Deep Sea Res. Part II Top. Stud. Oceanogr. 47, 1679–1700. https://doi.org/10.1016/S0967-0645(00)00003-5

Zhang, Y., 2015. Effects of temperature, carbonate chemistry and light intensity on the coccolithophores Emiliania huxleyi and Gephyrocapsa oceanica. University of Kiel.

Supporting Information for

Insolation forcing of coccolithophore productivity in the North Atlantic during the middle Pleistocene

C. Cavaleiro[1, 2, 3], A. H. L. Voelker[2, 3], H. Stoll[4*], K.-H. Baumann[1, 5], D. K. Kulhanek[6], B. D. A. Naafs[7], R. Stein[8], J. Grützner[8], C. Ventura[2], and M. Kucera[1]

[1] University of Bremen, MARUM - Center for Marine and Environmental Sciences, Leobener Straße 28359, Germany.

[2] IPMA – Instituto Português do Mar e da Atmosfera, Divisão de Geologia Marinha e Georrecursos Marinhos, Rua Alfredo Magalhães Ramalho 6, 1495-006 Lisboa, Portugal. [3] CCMAR, Centro de Ciências do Mar, Universidade do Algarve, Campus de Gambelas, 8005-139 Faro, Portugal. [4] Geology Department, University of Oviedo, C/. Jesús Arias de Velasco s/n, 33005, Oviedo, Spain. [5] University of Bremen, Geosciences Department, Klagenfurter Straße, 28359 Bremen, Germany. [6] International Ocean Discovery Program, Texas A&M University, College Station, Texas 77845-9547, USA. [7] Organic Geochemistry Unit, School of Chemistry, Cabot Institute, University of Bristol, Cantock's Close, Bristol BS8 1TS, UK. [8] Alfred-Wegener Institute for Polar and Marine Research, Am Alten Hafen 26, 27568 Bremerhaven, Germany. [*]now at: Department of Earth Sciences, ETH Zürich, Sonneggstrasse 5. 8092 Zürich, Switzerland

Contents of this file

This Supporting Information provides supplementary figures 1 and 2 (Fig. S1 and Fig. S2). Fig. S1 shows the IODP Site U1313 core photos along the primary and secondary splice, respectively, and information on the age model and sedimentation rates for the studied interval. Fig. S2 illustrates the location of samples for the coccolith assemblage counts relative to the Sr/Ca ratio and Sr/Ca residual curves.

Additional Text S1 and S2 containing Fig. S3 to S7 focus on the validity of the time-series analysis and on the methodology and reasoning for use of specific software, respectively. Supplementary Fig. S3 to Fig. S7 contain relevant spectral power results that support the main scientific conclusions of the paper but are not essential to the conclusions.

1145

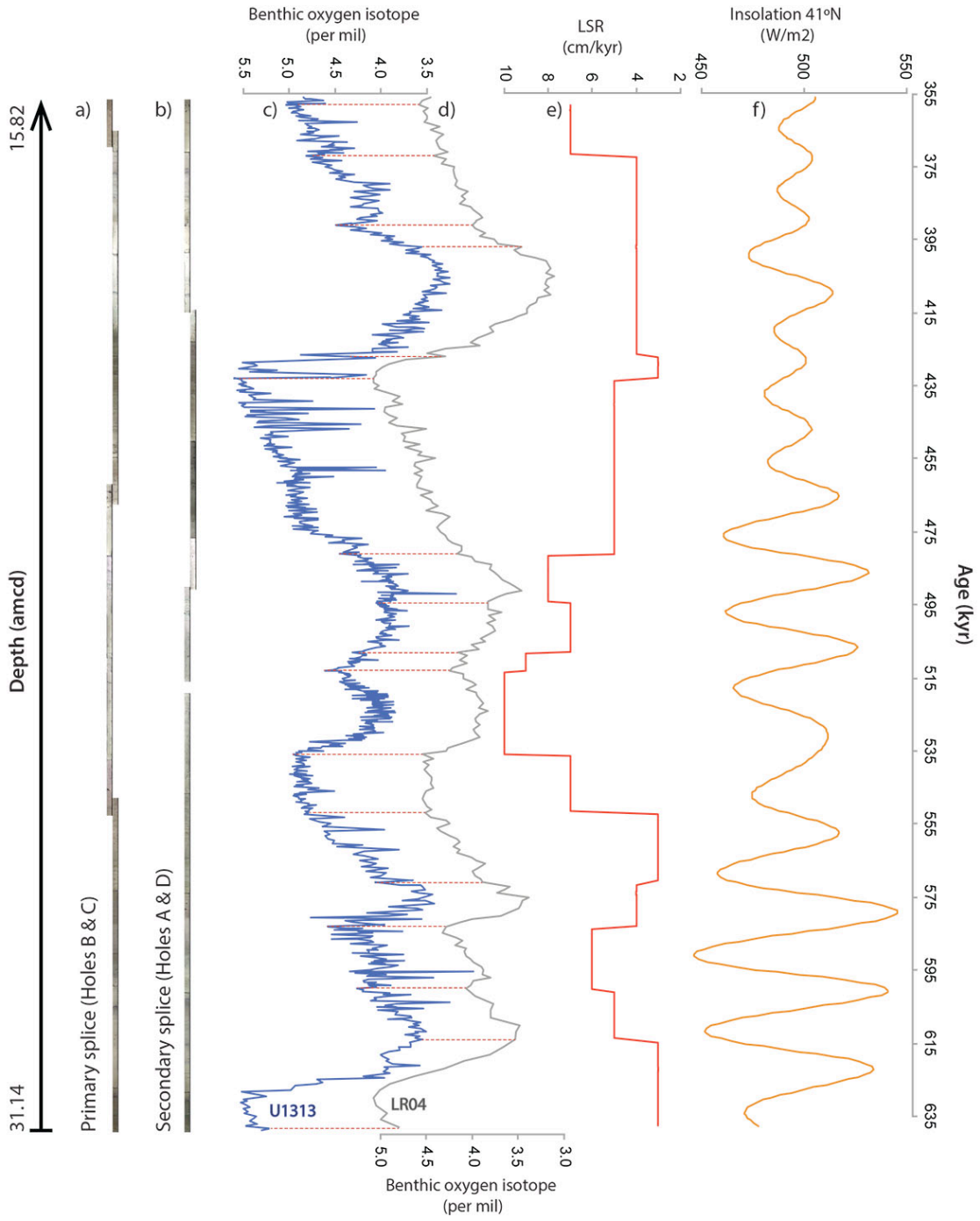

1146

1147 **Figure S1**. IODP Site U1313 splices and age model: a) primary and b) secondary splices (core photos), c) Site

1148 U1313 $\delta^{18}O_b$ (blue line; adjusted to Uvigerina $\delta^{18}O$ level; Stein et al., 2009; Voelker et al., 2010) and d) LR04 $\delta^{18}O_b$

1149 (grey line; adjusted to Uvigerina $\delta^{18}O$ level) (Lisiecki and Raymo, 2005), e) linear sedimentation rate (LSR, red line)

1150 and f) insolation at 41ºN (orange line) (Laskar et al., 2004)**.** Red dashed lines indicate tie points between the Site

1151 U1313 record and the LR04 stack.

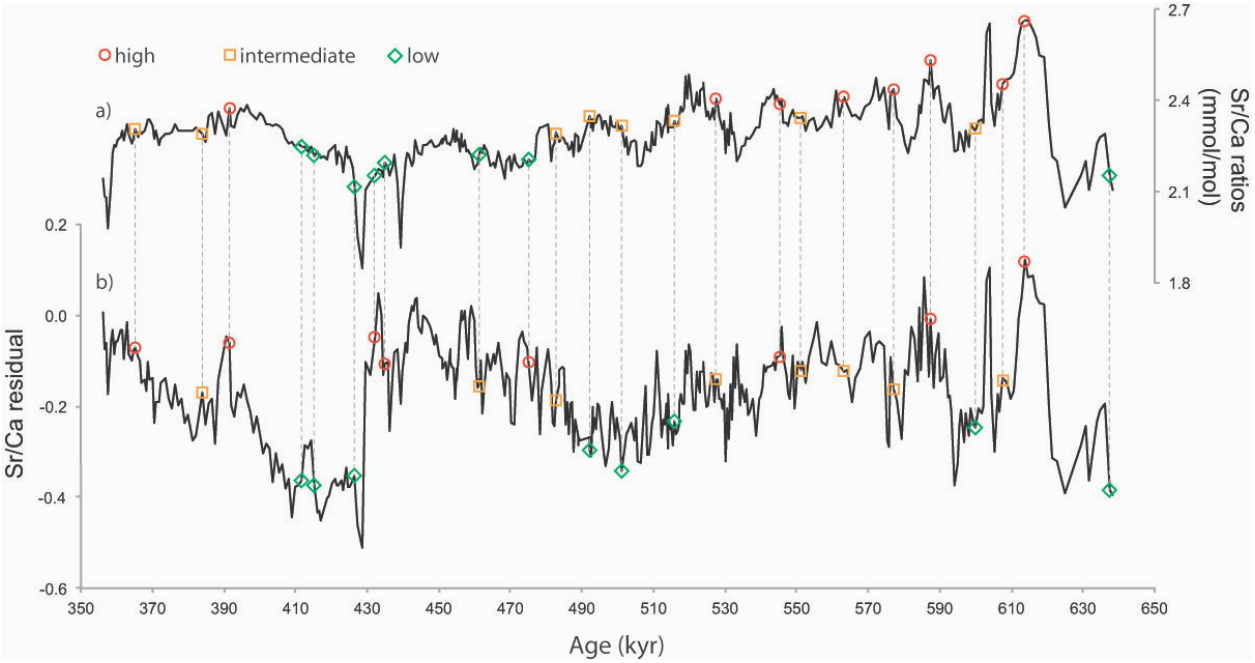

Figure S2. Location of coccolith assemblage samples: a) coccolith fraction Sr/Ca ratio results (mmol/mol), b) Sr/Ca residual curve; Red, orange and green dots indicate samples with high, intermediate and low Sr/Ca values, respectively; used for coccolith assemblage analyses.

Text S1. Time-series analysis validity

We here present the first coccolithophore paleoproductivity reconstruction for a mid-latitude area based on the coccolith fraction Sr/Ca ratio. Our record has the distinction of being from a geographical area that experienced abrupt temperature and ocean circulation changes. For example, the abrupt SST shift of approximately 10 ºC during Termination V (MIS 12 to MIS 11) or the shifts in deep-water mass fluctuations from North Atlantic Deep Water to the more carbonate-corrosive Antarctic Bottom Water during glacial MIS 12.

Despite the abrupt climatic changes, the following arguments convinced us that the reconstructed relative coccolithophore paleoproductivity variations are neither an artifact nor an over-correction of the temperature changes, and hence the time-series analysis is valid.

1) We aim to reconstruct coccolithophore productivity qualitatively in order to investigate the factors controlling it. For that we needed a continuous proxy to run time-series analysis. We investigated periodicities in the paleoproductivity data related to different climate system forcing. The TOC or the alkenone records are not constant throughout the record; during warmer periods, the organic matter content is almost negligible. Thus, we started by analyzing the CF Sr/Ca data and the coccolithophore productivity. We found significant periodicities at approximately 23 kyr and 15 kyr in both records. We then analyzed the $U^{k'}_{37}$ -based SST record and the alkenone content (despite not being continuous) to look for periodicities similar to the periodicities found in the coccolithophore productivity record. This was to determine if the dominant periodicities were an artifact of the temperature correction. In fact, neither the $U^{k'}_{37}$-based SST record nor the total alkenone concentration time-series analysis (Fig. S7a and b) show the 15 kyr periodicity found in the coccolithophore paleoproductivity data.

2) The alkenone content downcore can be used as a coccolithophore paleoproductivity proxy if there are no significant changes in the preservation/degradation of the organic matter through time, in the water column and in the sediment. However, a multiproxy approach is much more advisable than individual proxy analysis when reconstructing past conditions. Therefore, we also examined other commonly used productivity proxies, such as the nannofossil accumulation rate, total organic carbon, and total alkenone concentration and accumulation in the sediments. As stated in section 5.4 of the Discussion we combined the alkenone concentration, coccolith

preservation, coccolithophore paleoproductivity and carbonate content to conclude that coccolithophore productivity was relatively higher during glacials and lower during interglacials.

Therefore, despite similarities between the coccolithophore productivity curve and the $U^{k'}_{37}$ -based SST record, there is no evidence that it inherited its periodic characteristics due to temperature correction. Also, the coccolithophore paleoproductivity record still carries the same strong signals for the same periodicities as the original curve. Therefore, we assume that the coccolithophore productivity is not an artifact of the temperature correction and has its own periodic characteristics, worthy of being analyzed and discussed.

Text S2. Time-series analysis results and reasoning

The time series analysis tested for statistically significant periodicities in the coccolithophore productivity record. First, harmonic analyses were used to look for orbital periodicities in the coccolithophore productivity record. To further emphasize the suborbital scale variability (namely, precession and semi-precession signals) and to reduce the signal-to-noise ratio of coccolithophore productivity, several smoothing and filtering techniques were used. We then extracted the longer orbital periodicities (eccentricity and obliquity signals) using SPECTRUM and we further used a Gaussian bandpass filter with a central frequency of 0.01 cycles/kyr (10 kyr) and a bandwidth of 0.067 cycles/kyr (14 kyr) and Kernel smooth estimates (Mudelsee, 2014) centered at 23, 19 and 14 kyr, respectively, for comparison. Both Gaussian and Kernel curves were subtracted from the coccolithophore productivity time series and the resultant curves analyzed in REDFIT (the resultant filtered time series are shown in Fig. S3 and S4).

In detail, to reduce the signal-to-noise ratio of coccolithophore productivity, several smoothing and filtering techniques, using different available software, were performed prior to the time series analysis:

a) the Analyseries package was used for smoothing and filtering with the that it will only analyze evenly spaced time-series; so the record was first re-calculated to an evenly spaced resolution;

b) SPECTRUM was used for preliminary analyses, such as harmonic analysis, smoothing and filtering;

c) the Kernel package (Mudelsee, 2014) was used for smoothing and filtering;

d) the REDFIT package was used for spectral analysis of all original and resultant time series.

SPECTRUM was also used to perform cross-spectral analysis of the coccolithophore productivity record and the atmospheric carbon dioxide reconstruction by Lüthi et al. (2008).

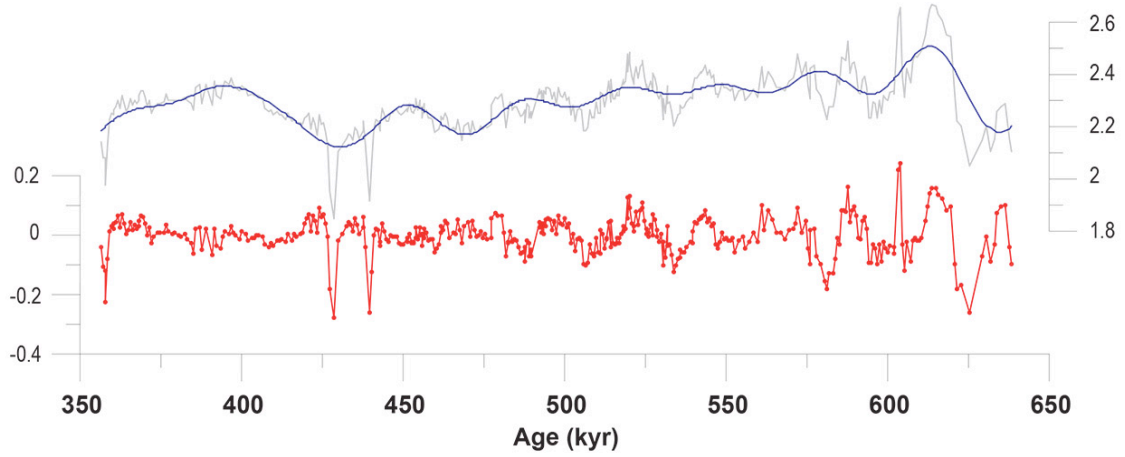

Figure S3. Original and filtered time series:

top) CF Sr/Ca ratio time series (grey) and smoothed curve (a) – b)) (blue);

bottom) CF Sr/Ca ratio filtered time series with SPECTRUM through harmonic analysis at **189**, **103**, **70.7**, **56.6**, **40.4**, **35.4** and **32.3** kyr (red).

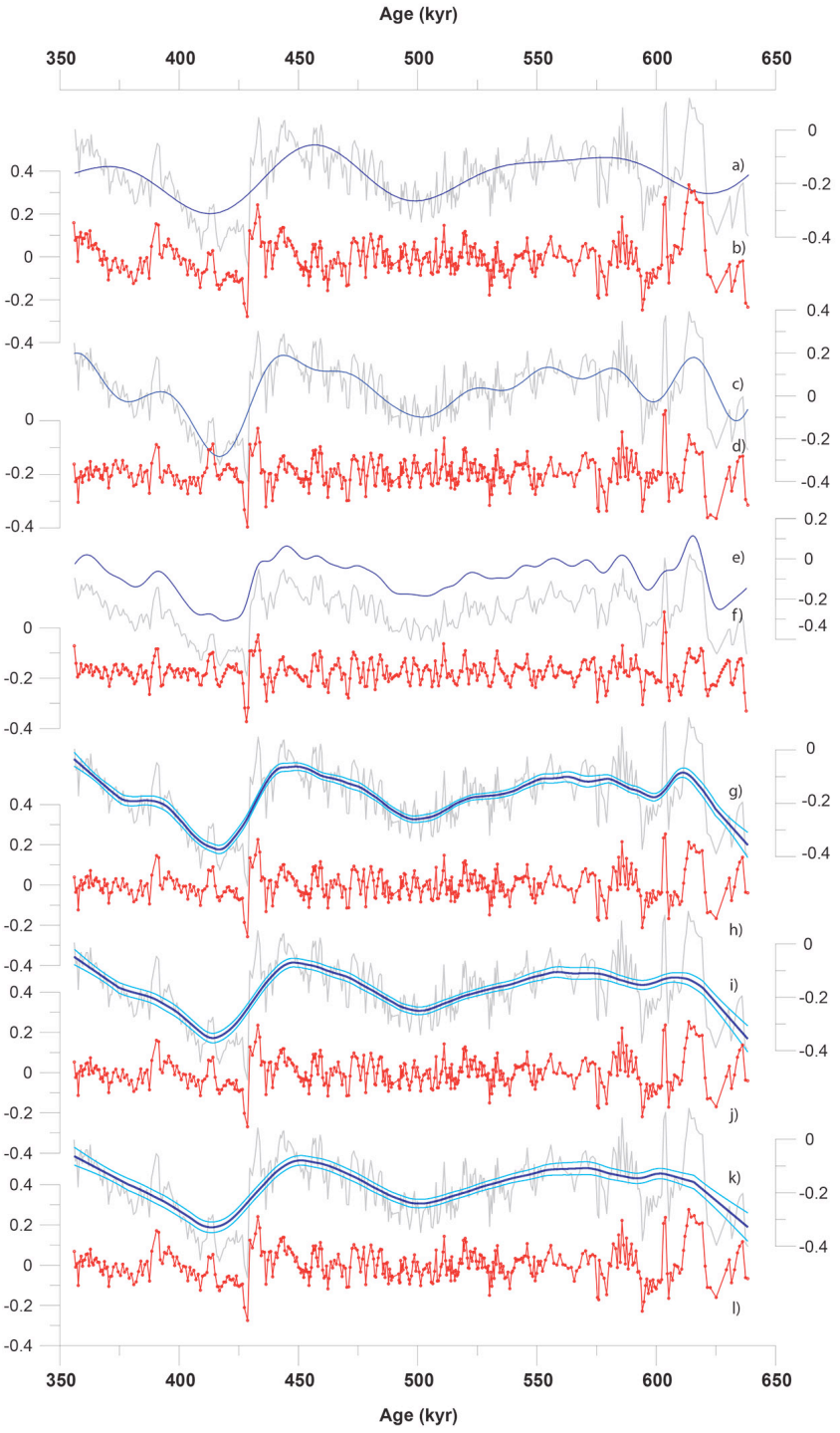

Figure S4. Original and filtered time series:

a) Coccolithophore productivity (CPP) time series (grey) and smoothed curve (CPP – b)) (blue);

b) CPP filtered time series with SPECTRUM through harmonic analysis at **126**, **94.3** and **70.55** kyr (red);

c) CPP time series (grey) and smoothed curve (CPP – d)) (blue);

d) CPP filtered time series with SPECTRUM through harmonic analysis at **189**, **126**, **94.3**, **70.55**, **62.9**, **51.4**, **43.6**, **36.5**, **32.3** and **29.8** kyr (red);

e) CPP time series (grey) and Gaussian curve produced in Analyseries (blue). The Gaussian bandpass filter used had a frequency of 0.01 c/kyr (10 kyr) and a bandwidth of 0.067 c/kyr (14 kyr);

f) CPP filtered time series (CPP – Gaussian curve) (red);

g) CPP time series (grey) and Kernel estimate smooth (dark blue) and correspondent lower and upper standard deviation (light blue lines) with a bandwidth of 14 kyr;

h) CPP filtered time series (CPP – Kernel estimate for 14 kyr) (red);

i) CPP time series (grey) and Kernel estimate smooth (dark blue) and correspondent lower and upper standard deviation (light blue lines) with a bandwidth of 19 kyr;

j) CPP filtered time series (CPP – Kernel estimate for 19 kyr) (red);

k) CPP time series (grey) and Kernel estimate smooth (dark blue) and correspondent lower and upper standard deviation (light blue lines) with a bandwidth of 23 kyr;

l) CPP filtered time series (CPP – Kernel estimate for 23 kyr) (red).

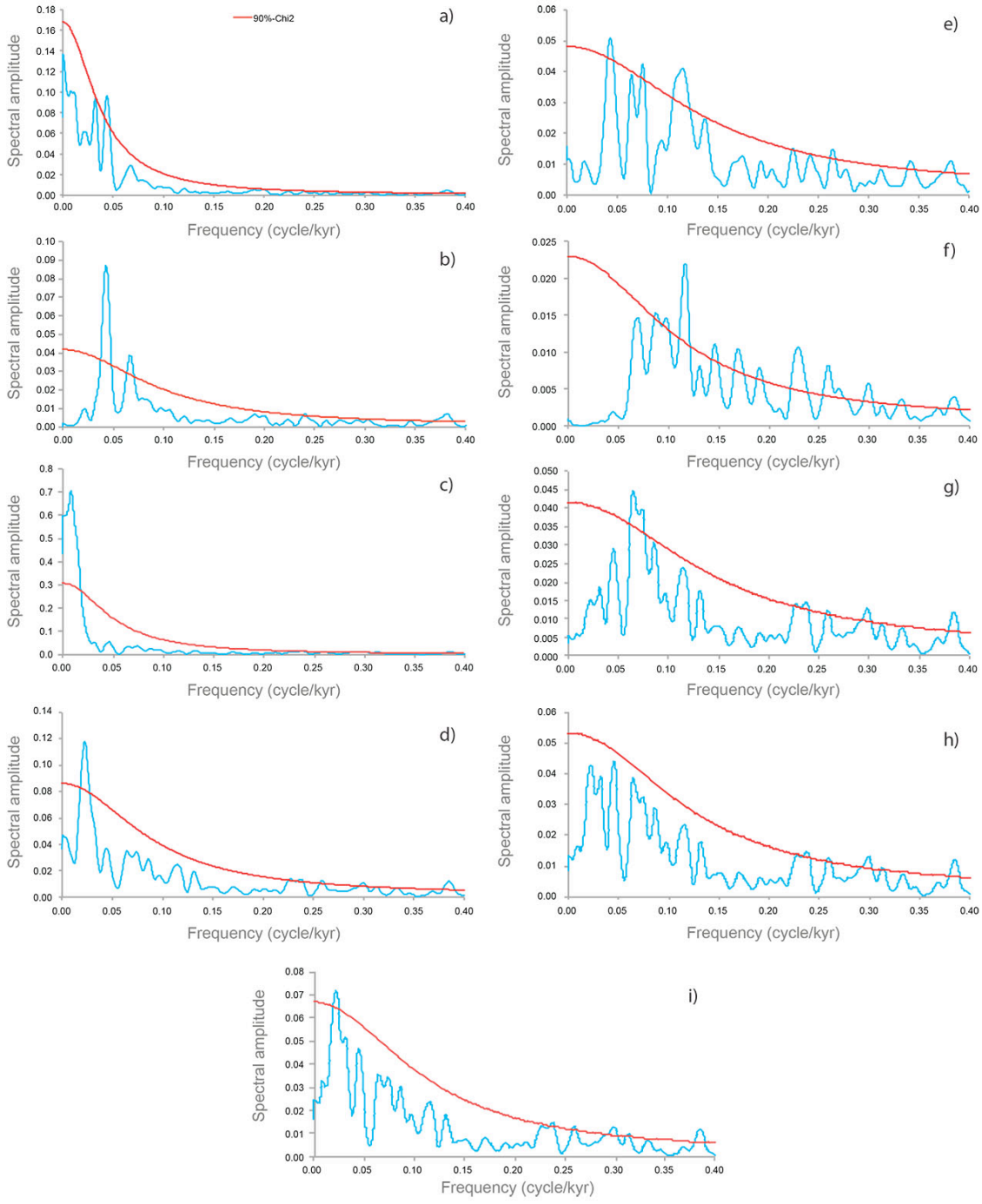

Figure S5. REDFIT spectral power results with 3 segments (50 % overlap) for each of the following time series:

a) CF Sr/Ca ratio (mmol/mol);

b) CF Sr/Ca ratio (mmol/mol) filtered with SPECTRUM through harmonic analysis at **103**, **70.7**, **40.4**, **56.6**, **332.3** and **35.4** kyr;

c) CPP;

d) CPP filtered with SPECTRUM through harmonic analysis at **126**, **94.3** and **70.55** kyr;

e) CPP filtered with SPECTRUM through harmonic analysis at **189**, **126**, **94.3**, **70.55**, **62.9**, **51.4**, **43.6**, **36.5**, **32.3** and **29.8** kyr;

f) CPP filtered with Analyseries by a Gaussian smoothing with a central frequency of 0.01 c/kyr and a bandwidth of 0.067 c/kyr;

g) CPP filtered with Kernel package by a Kernel smoothing for a cyclicity of 14 kyr;

h) CPP filtered with Kernel package by a Kernel smoothing for a cyclicity of 19 kyr;

i) CPP filtered with Kernel package by a Kernel smoothing for a cyclicity of 23 kyr.

The red line defines the significance level of 90% Chi2 (the peaks below this line correspond to cyclicities that are not significant). Bandwidth for the results with time series divided in 3 segments is 0.010.

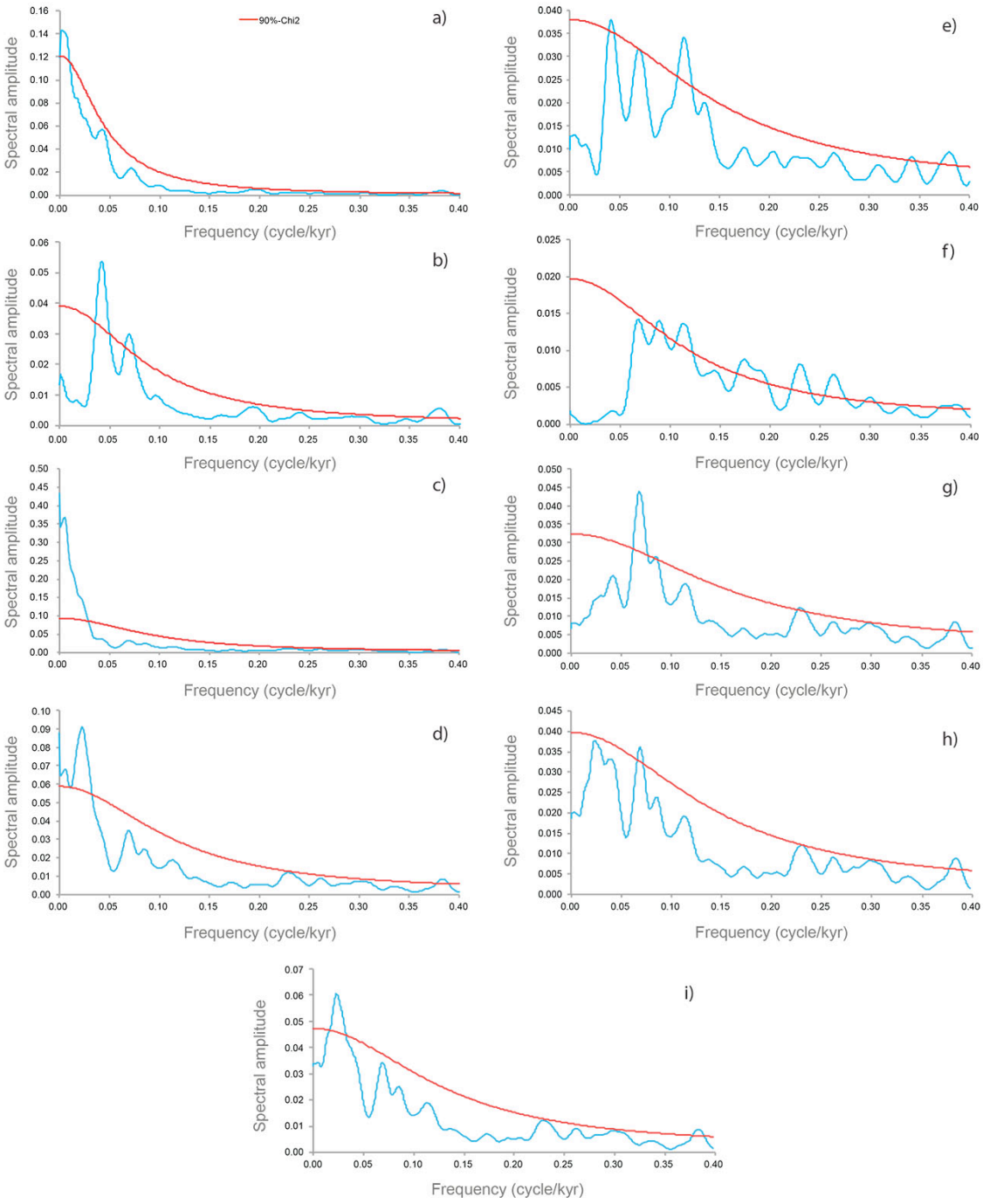

Figure S6. REDFIT spectral power results with 6 segments (50 % overlap) for each of the following time series:

a) CF Sr/Ca ratio (mmol/mol);

b) CF Sr/Ca ratio (mmol/mol) filtered with SPECTRUM through harmonic analysis at **103**, **70.7**, **40.4**, **56.6**, **332.3** and **35.4** kyr;

c) CPP;

d) CPP filtered with SPECTRUM through harmonic analysis at **126**, **94.3** and **70.55** kyr;

e) CPP filtered with SPECTRUM through harmonic analysis at **189**, **126**, **94.3**, **70.55**, **62.9**, **51.4**, **43.6**, **36.5**, **32.3** and **29.8** kyr;

f) CPP filtered with Analyseries by a Gaussian smoothing with a central frequency of 0.01 c/kyr and a bandwidth of 0.067 c/kyr;

g) CPP filtered with Kernel package by a Kernel smoothing for a cyclicity of 14 kyr;

h) CPP filtered with Kernel package by a Kernel smoothing for a cyclicity of 19 kyr;

i) CPP filtered with Kernel package by a Kernel smoothing for a cyclicity of 23 kyr.

The red line defines the significance level of 90% Chi2 (the peaks below this line correspond to cyclicities that are not significant). Bandwidth for the results with time series divided in 6 segments is 0.020.

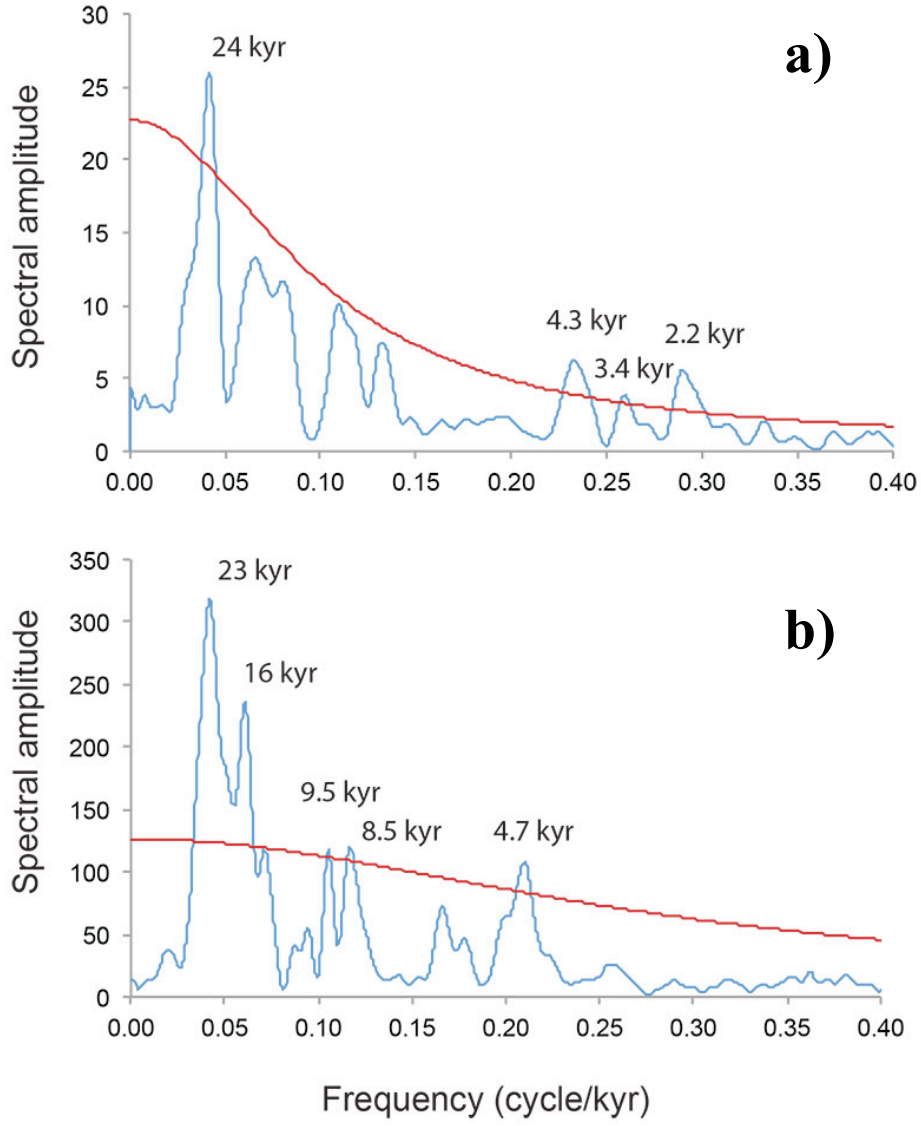

1271

1272 **Figure S7.** REDFIT spectral power results for the alkenone based sea-surface temperature curve ($U^{k'}_{37}$-based SST)
1273 and alkenone content records: a) $U^{k'}_{37}$-based SST record filtered with SPECTRUM through harmonic analysis (at
1274 103, 162, 80, 38.7, and 46.5 kyr) with 3 segments (50 % overlap); b) alkenone content record filtered with
1275 SPECTRUM through harmonic analysis (at 103, 232, 54.7, 77.4, 33.2, 61.9, 38.7 and 46.5 kyr) with 3 segments (50
1276 % overlap). The red line defines the significance level of 90% Chi2 (peaks below this line correspond to cyclicities
1277 that are not significant). Bandwidth for the results with time series divided in 3 segments is 0.010. The quasi-
1278 periodicities found are written on top of each spectral peak.